

# Geminet: Learning the Duality-based Iterative Process for Lightweight Traffic Engineering in Changing Topologies

Ximeng Liu, Shizhen Zhao, Xinbing Wang  
Shanghai Jiao Tong University

## ABSTRACT

Recently, researchers have explored ML-based Traffic Engineering (TE), leveraging neural networks to solve TE problems traditionally addressed by optimization. However, existing ML-based TE schemes remain impractical: they either fail to handle topology changes or suffer from poor scalability due to excessive computational and memory overhead. To overcome these limitations, we propose Geminet, a lightweight and scalable ML-based TE framework that can handle changing topologies. Geminet is built upon two key insights: (i) a methodology that decouples neural networks from topology by learning an iterative gradient-descent-based adjustment process, as gradient descent’s update rule is topology-agnostic, relying only on a few gradient-related quantities; (ii) shifting optimization from path-level routing weights to edge-level dual variables, reducing memory consumption by leveraging the fact that edges are far fewer than paths. Evaluations on WAN and data center datasets show that Geminet significantly improves scalability. Its neural network size is only 0.04% – 7% of existing schemes, while handling topology variations as effectively as HARP, a state-of-the-art ML-based TE approach, without performance degradation. When trained on large-scale topologies, Geminet consumes under 10 GiB of memory—over eight times less than HARP’s 80+ GiB—while achieving 5.45× faster convergence speed, demonstrating its potential for large-scale deployment.

## 1 INTRODUCTION

Both data center networks [5, 6, 10, 14, 16, 38, 45] and Wide Area Networks [8, 18, 19, 26–28, 31, 40, 44, 49, 52, 54] increasingly rely on traffic engineering (TE) to optimize network performance. TE, typically enabled by a centralized controller [3, 4, 11, 22, 23, 30, 32, 38, 53], solves optimization problems to efficiently route traffic across network paths.

Conventional TE schemes typically rely on optimization techniques, such as linear programming. However, as the scale of network topologies grows, conventional optimization methods struggle to swiftly adapt to traffic changes at fine time scales. Consequently, recent research has explored alternative approaches to design TE schemes based on neural network models [7, 34, 37, 52]. This shift is driven by the fact

that neural networks not only infer significantly faster than conventional models [52], but also have the potential to perform prediction and optimization jointly for better network performance [37] and handle traffic bursts [34].

Despite their promising potential, existing ML-based TE schemes face two critical challenges, which prevent their practical deployment in production environments: (i) *Handling variations in topology*. Network topologies continually change due to evolution, failures, or planned maintenance [7]. For ML-based TE schemes that cannot handle variations in topology, each change necessitates retraining, which increases operational costs and delays decision-making. Most ML-based TE schemes, such as DOTE [37], FIGRET [34], and TEAL [52], are not explicitly designed for such variations in topology, which limits their practical applicability. (ii) *Scalability in computational resource consumption and memory usage*. While some approaches, such as HARP [7], are designed to handle changing topologies, they face significant scalability challenges. As network size increases, the hardware requirements of HARP grow super-linearly, resulting in prohibitive memory consumption and extremely low throughput during training. To make things worse, the recurrent adjustment unit in HARP makes using multi-GPU deployment to alleviate scalability issues more costly and further reduces throughput. This is due to the frequent synchronization of data across GPUs required by the recurrent adjustment unit. This discourages network operators from adopting such approaches in production environments.

The reasons why there are no TE schemes that can handle changing topologies while maintaining high scalability can be summarized as follows: (i) The lack of a principled methodology for handling changing topologies forces existing approaches to rely on stacking neural network modules. However, these modules may generate a large amount of intermediate data during computation, leading to reduced throughput and increased memory consumption. (ii) TE requires computing split ratios for each path. However, in large-scale topologies, the number of paths is extremely large, as the number of source-destination pairs grows quadratically with the number of nodes, and each pair may have multiple paths. In existing ML-based TE schemes, these split ratios are generated using neural networks, but the sheer number

of paths either results in overly large models or an excessive number of intermediate variables, limiting scalability.

To tackle these challenges, we design Geminet, a light-weight and scalable ML-based TE scheme capable of handling changing topologies, with the promise of no compromise in TE decision performance. First, we propose a principled methodology for handling changing topologies—learning the gradient descent iterative process. Intuitively, the update rule of gradient descent is universal and can be applied to any topology. This inspires us to learn the iterative update rule itself rather than solving the entire TE problem directly. More specifically, gradient descent updates split ratios on paths, based on the derivative of the objective function with respect to these ratios. This update rule is topology-agnostic, as it depends only on gradient-related quantities, such as link utilization and traffic demand. Therefore, we use a neural network to learn the mapping between these gradient-related quantities and the adjustment of split ratios, which enables the neural network to remain decoupled from topology information. In fact, the relevant topology information is inherently captured in these gradient-related quantities, such as link utilization, which are simply inputs to this neural network. This allows Geminet to handle changing topologies without requiring additional neural network modules to explicitly process topology structure.

Through learning the gradient descent iterative process, Geminet can handle changing topologies without requiring additional modules. However, as mentioned earlier, when the topology grows, the number of paths increases significantly. If the model iterates over each path, it leads to excessive per-path computations, resulting in high memory and computation overhead. To address this, we harness duality theory and find that determining the optimal values of edge-based dual variables allows us to effortlessly obtain the solution to the original TE problem, i.e., the split ratios on paths. This enables a seamless transition from path-based to edge-based optimization. Theoretically, this approach transforms the iteration complexity from  $O(KN^2)$  at the path level to just  $O(N^2)$  at the edge level, where  $K$  is the number of paths per source-destination pair and  $N$  is the number of nodes. Even more favorably, since the total number of paths is always  $KN^2$ , open-source network topologies reveal that the actual number of edges is often far smaller than  $N^2$  (or more precisely,  $KN(N-1)$  for paths and  $N(N-1)$  for edges, as they typically exclude self-pairs and self-loops), making this approach even more efficient in practice.

We evaluate Geminet using publicly available WAN datasets, as well as data center PoD-level and ToR-level topologies and traffic data. Our key results are as follows: (i) Geminet’s ability to handle all topology variations is on par with HARP without any performance compromises. This holds for any scenarios, including the addition and removal

of nodes and links, changes in edge nodes, variations in link capacity (including link failures), and recomputation of tunnels. (ii) Geminet requires significantly fewer parameters, utilizing just 7% of TEAL’s, 2.6% of HARP’s, and 0.04% of DOTE’s. (iii) In large-scale topologies, where HARP’s training memory consumption exceeds 80 GiB, Geminet requires less than 10 GiB. The convergence speed is  $5.45\times$  faster than HARP’s. Additionally, Geminet’s inference time is  $2.3\times$  faster than HARP’s.

*This work does not raise any ethical concerns.*

## 2 BACKGROUND AND MOTIVATION

### 2.1 Background: ML-based TE

Given a network topology, a traffic matrix, and a set of paths TE schemes determine traffic routing on each path to optimize a desired network performance objective. A common widely used objective is the Maximize Link Utilization (MLU). Conventional TE systems are primarily based on linear programming algorithms.

Due to linear programming algorithms struggling to scale solution times with growing network sizes, researchers have recently begun to explore ML-based TE schemes. We introduce several representative ML-based TE schemes as follows:

**DOTE/FIGRET** [34, 37]: As illustrated in Figure 1(a), both DOTE and FIGRET employ a simple feedforward deep neural network (DNN) which receives a flattened traffic matrix as input and directly outputs the flattened split ratios. It has two limitations: (i) This approach does not model nodes, edges, link capacities, or paths, assuming these elements to be static. (ii) Additionally, the neural network is required to output the split ratios for all paths, the size of the neural network is directly related to the total number of paths.

**TEAL** [52]: As illustrated in Figure 1(b), TEAL models the topology using a bipartite graph of edges and paths, processed by FlowGNN. FlowGNN combines Graph Neural Network (GNN) layers to capture edge-path relationships and DNN layers to handle interactions among paths within the same flow. To address varying path counts caused by topology changes, TEAL employs a sharded MLP to process each source-destination pair independently, resolving input length issues and improving scalability. However, this approach has two key limitations: (i) it assumes a fixed set of paths for each source-destination pair, and (ii) processing source-destination pairs separately rather than concurrently may compromise TE performance.

**HARP** [7]: As illustrated in Figure 1(c), building on TEAL’s approach of processing source-destination pairs independently, which may be sensitive to path order, HARP processes each path independently to handle changing topologies. It uses a GNN to extract edge embeddings, which are input into a set transformer to compute path embeddings.



TE scheme	GEANT		Cogentco		Meta WEB DC		KDL		ASN	
	#Node 22, #Edge 72		#Node 197, #Edge 486		#Node 324, #Edge 12796		#Node 754, #Edge 1790		#Node 1739, #Edge 8558	
	Model Mem	Total Mem	Model Mem	Total Mem	Model Mem	Total Mem	Model Mem	Total Mem	Model Mem	Total Mem
DOTE/FIGRET	0.004	0.02	0.30	0.53	0.80	1.33	4.36	9.97	7.25	40.10
Teal	2.6e-5	0.02	2.6e-5	0.78	2.6e-5	1.48	2.6e-5	14.6	2.6e-5	43.49
HARP	7.3e-5	0.07	7.3e-5	18.8	7.3e-5	10.62	7.3e-5	>80	7.3e-5	>80
<b>Ours</b>	1.9e-6	0.02	1.9e-6	0.45	1.9e-6	0.99	1.9e-6	9.83	1.9e-6	20.50

**Table 1: Comparison of GPU memory usage for training across different topologies. The data in the Table is in GiB. Ours, i.e., Geminet, is proposed in §4 and evaluated in §5.**

For HARP, the state-of-the-art algorithm that supports variable topologies, training for deployment in large-scale topologies may require hundreds of gigabytes of GPU resources. To illustrate this, we summarize the memory usage of various ML-based TE algorithms in Table 1. The reported memory consumption is measured using the peak GPU memory allocation, as tracked by PyTorch’s built-in memory profiling tools. Training is conducted with a batch size of 16 and a data format of float32. The table presents two types of memory usage: (i) Model Mem, corresponding to the memory associated with neural network parameters, and (ii) Total Mem, representing overall GPU consumption. It can be seen that GPU usage depends not only on model size but also on additional intermediate variables generated during computation. Notably, HARP, when trained on a topology with 754 nodes and 1,790 edges, occupies over 80 GiB of memory, with inference memory demands reaching 71.85 GiB. We exclude RedTE from the table because its memory consumption exceeds 80 GiB on all but the smallest topologies (e.g., GEANT), making it impractical to profile under consistent settings. Instead, in §5.6, we provide a theoretical analysis of RedTE’s neural network memory usage to illustrate the root cause of its excessive training overhead.

**Adding more hardware resources is not a cost-effective solution.** Simply increasing hardware resources is not an efficient way to address this issue for two main reasons. First, hardware demand grows super-linearly with network size, making this approach unsustainable. Real-world networks can be much larger than the topology discussed earlier. For instance, the WAN topology of a global cloud provider in [52] contains 1,739 nodes and 8,558 edges, making hardware-based scaling a bottomless pit. Second, even with sufficient hardware, HARP’s architecture complicates distribution across multiple GPUs. Existing parallelization techniques, such as tensor parallelism (splitting within layers) and pipeline parallelism (splitting between layers) [42], become less efficient due to HARP’s RAU process. In tensor parallelism, assigning different paths to different GPUs requires frequent aggregation of TE decisions to compute MLU, leading to substantial inter-GPU synchronization overhead. Similarly, pipeline parallelism suffers from repeated

inter-GPU data transfers. Since the shared RAU requires iterative computations, each iteration involves sending data to the later segment for processing and then back to the earlier segment to prepare for the next iteration, introducing significant communication overhead. As a result, distributing HARP across multiple GPUs is complex and inefficient, making hardware expansion impractical. In contrast, our approach can be implemented on a single GPU due to its low memory usage, eliminating costly multi-GPU coordination.

**Reasons for poor scalability.** To understand the reasons for poor scalability, we first outline the key sources of memory consumption in neural network training [43]. These include model memory, which stores the neural network’s parameters; optimizer memory, which holds gradients and momentum buffers; and activation memory, which stores intermediate values required during backpropagation, including the outputs of each layer in the forward pass and their corresponding gradients in the backward pass. Thus, memory consumption is influenced not only by model size but also by the intermediate variables generated during computation. Based on this, the scalability limitations of existing approaches can be attributed to two main factors: (i) Stacking modules to handle changing topologies. Methods using graph neural networks for topology modeling or transformers for path embeddings introduce considerable computational overhead. For instance, self-attention in transformers processes each path individually, generating intermediate variables that scale quadratically with path length (see Appendix C.1 for details). (ii) The burden of optimizing large path outputs. As network size increases, the number of paths grows significantly. A network with  $N$  nodes contains  $N(N - 1)$  source-destination pairs, each with  $K$  available paths, resulting in a total of  $KN(N - 1)$  paths. Schemes like DOTTE, which directly output TE decisions for all paths, require large models due to high-dimensional outputs, while iterative approaches like HARP generate excessive intermediate variables due to the need for per-path adjustments.

### 2.3 Insights to improve scalability

**Decoupling topology-related parameters from neural networks.** Given the computational and memory overhead of handling topology within neural networks, we ask: can topology be decoupled from the neural network? Fortunately, the gradient descent update rule is inherently topology-agnostic, relying only on a few gradient-related quantities—such as link utilization and traffic demand—rather than explicit topology structures. This leads to our insight: instead of solving TE decisions directly, we use the neural network to learn the iterative adjustment process, mapping these gradient-related quantities to split ratio updates.

**Leveraging duality to shift from path-based to edge-based optimization.** The total number of paths in a network is large, making direct path-level TE decisions memory-intensive. However, as shown in Table 1, the number of edges is significantly smaller. Even in the extreme case of a fully connected graph, the number of edges remains only  $\frac{1}{K}$  of the total number of paths, where  $K$  is the number of paths per source-destination pair. This observation motivates us to explore whether duality theory can transform path-level TE optimization into solving dual variables associated with edges, significantly reducing memory consumption.

## 3 MODEL

**Notations & Definitions.** We introduce recurring mathematical notations and definitions of TE. All notations used in this paper are also tabulated in Table 3 for ease of reference.

- **Network.** Network topology is represented as a graph  $G(V, E, c)$ , where  $V$  and  $E$  are the node and edge sets, respectively, and  $c : E \rightarrow \mathbf{R}^+$  assigns capacities to edges.
- **Traffic demands.** A demand matrix  $D$  is of size  $|V| \times |V|$ , where  $D_{st}$  represents the traffic demand from  $s$  to  $t$ .
- **Paths.** Each source  $s$  communicates with each destination  $t$  via a set of network paths  $P_{st}$ .
- **TE configurations.** A TE configuration  $\mathcal{R}$  specifies for each path  $p \in P_{st}$  a split ratio  $r_p$ , where  $r_p$  is the fraction of the traffic demand from  $s$  to  $d$  forwarded along path  $p$ . The split ratios must satisfy  $\sum_{p \in P_{sd}} r_p = 1$ .
- **TE objective.** We focus on Maximum Link Utilization (MLU), a widely used TE metric [9, 10, 17, 38, 48], for concreteness. Google found MLU to be a reasonable proxy metric, as high MLU often signals imminent link overloads that lead to packet loss, longer flow completion times, and reduced throughput [38]. Given a demand matrix  $D$  and TE configuration  $\mathcal{R}$ , the total traffic traversing an edge  $e$  is  $f_e = \sum_{s,t \in V} \sum_{p \in P_{st}, p \ni e} D_{st} r_p$ , and then the MLU induced by  $D$  and  $\mathcal{R}$  is  $\max_{e \in E} \frac{f_e}{c(e)}$ . The extensibility to other objectives is discussed in §6.

**TE model.** Given the above definitions, Traffic Engineering optimization can be formulated in the form of Equation (1):

$$\begin{aligned}
 & \underset{\mathcal{R}, m}{\text{minimize}} && m \\
 & \text{subject to} && \sum_{s,t \in V} \sum_{p \in P_{st}, p \ni e} D_{st} \cdot r_p \leq m \cdot c(e), \quad \forall e \in E, \\
 & && \sum_{p \in P_{st}} r_p = 1, \quad \forall s, t \in V, \\
 & && r_p \geq 0, \quad \forall s, t \in V, p \in P_{st}.
 \end{aligned} \tag{1}$$

**Types of ‘variables’ in topologies.** Similar to [7], we categorize the ‘variables’ in topologies into the following types: (i) Variables in Node/Edge. This includes the addition or removal of nodes/edges, as well as the reordering of node/edge IDs in the graph. (ii) Variables in Path. This includes the re-selection of paths (i.e., the edges traversed change), as well as the reordering of path IDs within a source-destination pair. (iii) Variables in Capacity. The network topology remains unchanged, but the capacities of the edges vary.

**Objective of this work.** The objective of this work is to propose an ML-based TE scheme that 1) can handle changing topologies and 2) is lightweight, with low resource consumption and memory usage.

## 4 DESIGN

In this section, we present the design of Geminet. In §4.1, we propose a methodology for handling changing topologies without stacking neural networks to process topology: Learning the Iterative Process. Next, considering the excessive number of paths, we leverage duality theory in §4.2 to transform path-level iterations into edge-level iterations. Then, in §4.3, we introduce the framework of Geminet. Finally, in §4.4, we describe an optional approach to further improve scalability: training on sub-traffic matrices.

### 4.1 Learning the iterative process

We propose a methodology to equip TE with the capability to handle changing topologies by leveraging neural networks to learn the iterative optimization process, rather than directly solving the TE problem. This approach enables the decoupling of neural networks from topology information, eliminating the need to stack additional modules to handle topology complexities. The iterative process can be applied to either the primal or dual variables. In this section, we use the primal variables as an example for ease of understanding.

If we denote the optimization objective by Equation (1) as  $M(\mathcal{R})$ , and assume an initial solution  $\mathcal{R}$  is given, the gradient descent method can be used to iteratively update  $\mathcal{R}$  towards the optimal solution. For any  $r_p$  in  $\mathcal{R}$ , the update can be performed according to Equation (2), where  $\alpha$  represents the

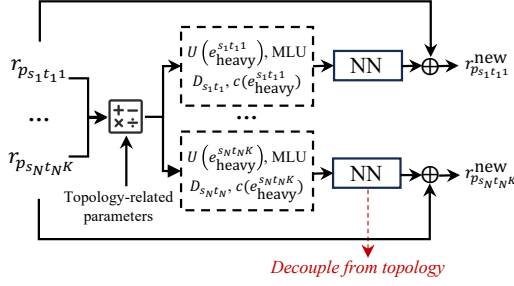


**Figure 2: Illustrating the iterative learning process: The neural network (NN) is decoupled from topology, with topology information fused into variables through simple mathematical operations before input to the NN.**

step size:

$$r_p^{\text{new}} = r_p - \alpha \frac{\partial M(\mathcal{R})}{\partial r_p}. \quad (2)$$

Here,  $\frac{\partial M(\mathcal{R})}{\partial r_p} = \frac{D_{st}}{c(e)}$  if the path  $p$  includes a link  $e$  whose Utilization  $(e) = \frac{\sum_{s,t \in V} \sum_{p \in P_{st}, p \ni e} D_{st} \cdot r_p}{c(e)}$  equals the MLU  $m$ ; otherwise,  $\frac{\partial M(\mathcal{R})}{\partial r_p} = 0$ . Specifically, based on Equation (2) and the computation of  $\frac{\partial M(\mathcal{R})}{\partial r_p}$ , the update of  $r_p$  depends only on the following four quantities: (i) the utilization of the most heavily utilized link on the path  $U(e_{\text{heavy}})$ , (ii) the global maximum link utilization MLU, (iii) the traffic demand flowing through the path  $D_{st}$ , and (iv) the capacity of the most heavily utilized link  $c(e_{\text{heavy}})$ . Therefore, Equation (2) can be rewritten in the form of Equation (3).

$$r_p^{\text{new}} = r_p - f(U(e_{\text{heavy}}), \text{MLU}, D_{st}, c(e_{\text{heavy}})) \quad (3)$$

We use a neural network to learn the function  $f$ , which takes the four quantities  $U(e_{\text{heavy}})$ , MLU,  $D_{st}$ ,  $c(e_{\text{heavy}})$  as input and outputs the adjustment for  $r_p$ . It can be observed that  $f$  is decoupled from the topology. Specifically, its inputs  $U(e_{\text{heavy}})$ , MLU,  $c(e_{\text{heavy}})$  represent topology-related information, but these inputs can be obtained through simple calculations. The mapping from these inputs to the adjustment of  $r_p$  by the function  $f$  does not need to consider the topology. Therefore, if a neural network is used to learn  $f$ , this decoupling allows the neural network to remain simple, and a straightforward multilayer perceptron (MLP) is sufficient to solve the problem.

The process of learning the iterative update, how it decouples the neural network from topology information, and how topology information is incorporated through simple computations is illustrated in Figure 2.

## 4.2 Harnessing duality

As mentioned, the iterative process can be applied to either the primal variables or the dual variables. Considering that the number of primal variables  $r_p$  in the TE problem is  $KN(N-1)$ , where  $N$  is the number of nodes, iterating over the primal variables would result in a large number of intermediate variables, leading to higher memory usage and increased computational resource consumption. Therefore, in this section, we leverage duality theory to transform the iteration over the primal variables into an iteration over the dual variables associated with edges. The maximum number of edges is  $N(N-1)$ , and as shown in the topology details in Table 1, the actual number of edges is often much smaller, significantly reducing the intermediate variable count and thereby decreasing memory usage.

**Formulate the Lagrangian relaxation.** For the optimization problem defined by Equation (1), the constraints  $\sum_{p \in P_{st}} r_p = 1, \forall s, t \in V$  and  $r_p \geq 0, \forall s, t \in V, p \in P_{st}$  can be easily satisfied through normalization [34]. Consequently, we apply a Lagrangian relaxation solely to the first constraint. To do this, we introduce a Lagrangian multiplier vector  $\lambda$  (where  $\lambda \in \mathbb{R}^{|E|}$ ) and formulate the Lagrangian relaxation as Equation (4). At this stage, the feasible region  $\mathcal{R}_{\text{feas}}$  for  $\mathcal{R}$ , defined by  $\mathcal{R}_{\text{feas}} = \{\mathcal{R} \in \mathbb{R}^{KN^2} \mid \sum_{p \in P_{st}} r_p = 1, \forall s, t \in V, \text{ and } r_p \geq 0, \forall s, t \in V, p \in P_{st}\}$ .

$$\begin{aligned} L(\mathcal{R}, m, \lambda) &= m + \sum_{e \in E} \lambda_e \left( \sum_{s,t \in V} \sum_{p \in P_{st}, p \ni e} D_{st} r_p - m \cdot c(e) \right) \\ &= \left( 1 - \sum_{e \in E} \lambda_e c(e) \right) m + \sum_{e \in E} \sum_{s,t \in V} \sum_{p \in P_{st}, p \ni e} \lambda_e D_{st} r_p \\ &= \left( 1 - \sum_{e \in E} \lambda_e c(e) \right) m + \sum_{s,t \in V} \sum_{p \in P_{st}} \sum_{e \in p} \lambda_e D_{st} r_p. \end{aligned} \quad (4)$$

The transition from the second to the third line in Equation (4) involves swapping the order of summation. For more details, please refer to Appendix B.1.

**Derive the primal optimal from the Lagrangian relaxation.** Since the primal problem is a linear programming problem, the optimal solution for  $\mathcal{R}$  can be directly obtained by optimizing the Lagrangian function, as shown in Equation (5), where  $\lambda^*$  is the optimal solution of  $\lambda$ . Related knowledge of dual theory is provided in Appendix B.3.

$$\underset{\mathcal{R}, m}{\text{minimize}} \left\{ L(\mathcal{R}, m, \lambda^*) \mid \mathcal{R} \in \mathcal{R}_{\text{feas}} \right\}. \quad (5)$$

Since only the second term involves  $\mathcal{R}$  in Equation (4), it can be rewritten in the form of Equation (6).

$$\underset{\mathcal{R}, m}{\text{minimize}} \left\{ \sum_{s,t \in V} \sum_{p \in P_{st}} \sum_{e \in p} \lambda_e^* D_{st} r_p \mid \mathcal{R} \in \mathcal{R}_{\text{feas}} \right\}. \quad (6)$$

Furthermore, the optimization problem specified in Equation (6) can be rewritten as minimize  $\mathcal{R}, m \left\{ \sum_{s,t \in V} D_{st} \sum_{p \in P_{st}} (\sum_{e \in p} \lambda_e^*) r_p \mid \mathcal{R} \in \mathcal{R}_{\text{feas}} \right\}$ . This reformulation shows that the objective function and the feasible region constraint are *independent* for each source-destination pair  $(s, t)$ . Given this structuring, we can decouple the optimization for each source-destination pair under the premise of maintaining optimality. The optimization problem for each pair can be formulated as in Equation (7).

$$\begin{aligned} & \text{minimize}_r && \sum_{p \in P_{st}} D_{st} (\sum_{e \in p} \lambda_e^*) r_p \\ & \text{subject to} && \sum_{p \in P_{st}} r_p = 1, r_p \geq 0, \forall p \in P_{st}. \end{aligned} \quad (7)$$

The solution to Equation (7) is remarkably simple. Since the  $D_{st}$  can be treated as a constant, it can be temporarily set aside. The objective  $\sum_{p \in P_{st}} (\sum_{e \in p} \lambda_e^*) r_p$  is minimized when all the weight is placed on the path  $p \in P_{st}$  with the smallest  $\sum_{e \in p} \lambda_e^*$ . This leads to the optimal solution: assign  $r_p = 1$  to the path with the smallest  $\sum_{e \in p} \lambda_e^*$ , while setting  $r_p = 0$  for all other paths.

In deep learning training, we implement this optimization by applying the Softmin operation to  $\sum_{e \in p} \lambda_e^*$  across all paths  $p \in P_{st}$ . The Softmin operation transforms the values  $\sum_{e \in p} \lambda_e^*$  into a probability distribution, where larger values result in smaller probabilities while ensuring that the sum of probabilities equals 1. Compared to direct minimization, this provides a smooth and differentiable approximation suitable for deep learning. For a detailed explanation of the Softmin operation, please refer to Appendix C.3.

**Iterative process on dual variables.** By now, we know that as long as the optimal dual variables can be obtained, the optimal splitting ratio can be easily determined. Therefore, the next question is how to adjust the dual variables using the iterative approach described in §4.1. To address this, we first compute the derivative of the Equation (4) to the dual variable. For any  $\lambda_e$ , the derivative is given in Equation (8).

$$\frac{\partial L}{\partial \lambda_e} = \sum_{s,t \in V} \sum_{p \in P_{st}, p \ni e} D_{st} r_p - m \cdot c(e). \quad (8)$$

$$\lambda_e^{\text{new}} = \lambda_e - f_{\text{Dual}}(F(e), \text{MLU}, c(e)). \quad (9)$$

From Equation (8), given  $\lambda$ , we first compute the corresponding  $\mathcal{R}$  using summation and Softmin operations. Next, we construct a neural network to learn  $f_{\text{Dual}}$  in Equation (9), taking as input: (i) the flow passing through the edge  $F(e)$ , (ii) the MLU, and (iii) the edge capacity  $c(e)$ . The network then outputs the adjustment for  $\lambda_e$ . The pseudocode for this method is provided in Pseudocode 1 in Appendix C.3.

### 4.3 Framework design

**Initial dual variable generation module design.** We first design how to solve for the initial dual variable. While any initial value converges to the optimal solution after sufficient gradient descent iterations, a well-chosen one can reduce the iterations required. The selection method is not unique, and we adopt a heuristic approach.

As can be seen from Equation (7),  $\lambda$  can be interpreted physically as the "congestion price". When the "congestion price" on a path ( $\sum_{e \in p} \lambda_e$ ) is too high,  $r_p$  should be smaller to avoid excessive network congestion. Therefore, the overarching idea for determining the initial value is that this value should reflect a certain degree of congestion.

Our approach is as follows: For each path, we use a neural network that receives the traffic flow for the source-destination pair it serves, along with the bottleneck edge capacity ( $\min_{e \in p} c(e)$ ) of that path. It outputs a potential load value for each path, forming a potential load vector  $\Psi^{(|\Phi|,1)}$ , where  $\Phi$  denotes the set of all paths. Subsequently, the potential loads of the paths passing through each edge are aggregated to determine the "potential load" for each edge, which can be computed by calculating  $\Psi^{(|\Phi|,1)} \times \xi^{(|\Phi|,|E|)}$ , where  $\xi^{(|\Phi|,|E|)}$  is the path-to-edge matrix, and  $\xi_{i,j} = 1$  indicates that path  $i$  contains edge  $j$ .

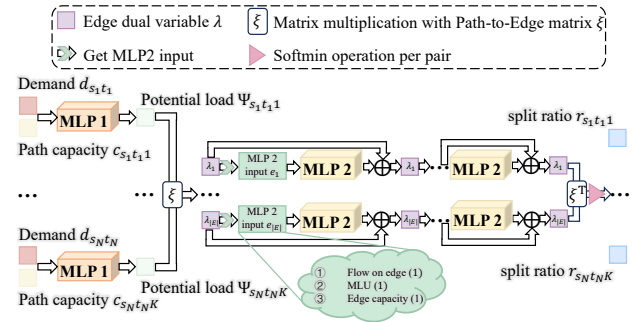


**Figure 3: Illustration of Geminet’s overall framework, which can be divided into two parts: the Initial Dual Variable Generation Module and the Adjustment Module. All modules with the same labels (MLP 1, MLP 2) share the same parameters.**

**Overall framework of Geminet.** By integrating the Initial Dual Variable Generation Module with the Adjustment Module, we establish the overall framework of Geminet, as depicted in Figure 3. Geminet uses MLU as the loss function, which is calculated based on Geminet’s output split ratios, along with the topology and traffic matrix. From the framework, it is evident that Geminet’s advantages not only include (i) the ability to handle changing topologies and (ii) being lighter and more scalable, but also offering greater interpretability. Each step in Geminet is clearly defined, making

it more interpretable than fully connected network structures like DOTE/FIGRET.

#### 4.4 Training on sub-traffic matrices

**How to partition the traffic matrix.** Since we learn the iterative adjustment process, which is independent of the structure of the traffic matrix, we can partition the traffic matrix into sub-traffic matrices to further reduce memory consumption. This involves splitting the source-destination (SD) pairs into multiple subsets and training on these sub-traffic matrices. More specifically, given a topology  $G(V, E)$  with  $|\Omega|$  SD pairs, each with  $K$  paths, the Path-to-Edge matrix has dimensions  $(K|\Omega|, |E|)$ , and the TE configuration has dimensions  $(K|\Omega|, 1)$ . Then, while keeping the topology unchanged, we divide the traffic matrix into  $S$  sub-traffic matrices, each containing  $|\Omega|/S$  SD pairs. Consequently, the dimensions of the Path-to-Edge matrix and TE configuration become  $(K|\Omega|/S, |E|)$  and  $(K|\Omega|/S, 1)$ , respectively. Importantly, we partition only the traffic matrix and not the topology itself. Figure 13 in Appendix C.4 illustrates an example of partitioning to aid understanding.

**Benefits of partitioning.** Partitioning reduces activation memory and memory consumption from sparse matrix multiplications. Since only a subset of the original traffic matrix is processed, fewer paths are included, leading to lower activation memory. Additionally, smaller sparse matrices require less memory for computation. For example, on KDL data, setting  $S = 4$  reduces sparse matrix multiplication memory overhead by 75.17% (see Appendix D.1).

**Why partitioning works.** From Equation (8), adjusting  $\lambda_e$  depends on the difference between edge utilization and the MLU, rather than absolute edge load. Since partitioning only affects absolute edge loads, it does not impact the iterative adjustment process. To ensure consistency between training (on sub-traffic matrices) and inference (on the full traffic matrix), we apply a normalization technique: instead of using absolute edge flow and MLU as separate inputs, we use the ratio of edge utilization to MLU, keeping data within  $[0, 1]$ . Evaluations in Appendix D.5 further confirm that both the distribution of MLP2’s input (the ratio of edge utilization to MLU) and the trained neural network parameters remain highly similar before and after partitioning.

## 5 EVALUATION

In this section, we first describe our evaluation methodology in §5.1. §5.2 then compares Geminet with HARP, the state-of-the-art TE scheme capable of handling changing topologies, and demonstrates that Geminet reduces memory usage and improves convergence speed without compromising performance. We further compare Geminet with other ML-based TE schemes that do not adapt to topology changes in §5.3,

considering scenarios where the network topology remains structurally unchanged, though paths may be shuffled. §5.4 evaluates Geminet’s ability to handle link failures. The effectiveness of our training on sub-traffic matrices strategy, introduced in §4.4, is examined in §5.5. We also evaluate Geminet’s performance under traffic uncertainty in §5.6 and compare the solution time across different TE schemes in §5.7. Finally, §5.8 shows that Geminet, having fewer parameters, requires less training data. In the appendix, besides supplementary results for the above evaluations, Appendix D.2 shows that the duality theory also applies to DOTE.

### 5.1 Methodology

We evaluate Geminet using real-world datasets and compare Geminet with state-of-the-art ML-based traffic engineering schemes. For detailed information about the evaluation setup, including machine specifications, CUDA version, and other configurations, please refer to Appendix C.5.

**Topologies.** Before delving into topology, we first define the categories of topological changes. A snapshot of a topology includes (i) the complete set of nodes and edges; and (ii) the capacities of the edges [7]. Consistent with [7], we define a “cluster” as a group of topologies where the set of nodes and edges is the same. A topology is classified as a One-cluster topology if its nodes and edges remain unchanged across all snapshots; otherwise, it is a Multi-cluster topology. Our evaluation tests both cases.

For one-cluster topologies, we evaluate our approach on a diverse set of real-world networks. For WANs, we include the pan-European research network GEANT [47] and two topologies from the Internet Topology Zoo [29]: Cogentco and KDL. For the AS-level Internet topology, we use the ASN topology [13], representing inter-AS connections at the BGP level. For data center (DC) topologies, we adopt the Meta WEB DC topology [41], which primarily handles web traffic. Within this DC, we consider both the Top-of-Rack (ToR) and Point-of-Delivery (PoD) levels. Since traffic engineering (TE) is rarely used in traditional Clos architectures, we instead employ a direct-connect topology [34]. At the PoD level, we use a fully connected network, while at the ToR level, we construct a random regular graph where nodes are connected based on a predefined probability.

For multi-cluster topologies, we evaluate on DynGeant, a dynamic variant of GEANT that evolves over time through changes in topology and link capacities. Since the HARP dataset is not publicly available, we construct DynGeant with dynamic characteristics similar to those described in HARP [7]. The topological variations of DynGeant are visualized in Appendix C.7, specifically in Figure 14 and Figure 15.

For each cluster, we use Yen’s algorithm to precompute the 4 shortest [31] paths between each source-destination pair, serving as the candidate paths for flow allocation.

**Traffic data.** For the GEANT topology, we utilize publicly available traffic matrix traces that consist of data aggregated every 15 minutes over four months [47]. In the case of the Meta topology, the data includes a public trace of one day’s traffic [41]. At the Pod level, we aggregate traces into 1-second intervals for the inter-pod traffic matrix, while for the ToR level, the aggregation interval is set at 10 seconds [34]. The longer intervals at the ToR level are necessary due to the larger topology involving more nodes, which results in greater computational and storage demands for TE [34]. For the Cogentco and KDL from Topology Zoo, no open-source dataset is available; thus, we employ the gravity model [8, 39] to generate traffic. The same approach is applied to ASN. When considering DynGeant, while we continue to rely on the publicly available data from GEANT, if node additions result in new source-destination pairs, we also apply the gravity model to generate the traffic. Unless otherwise specified, we use 75% of the data for training and 25% for testing.

**Metrics.** (i) TE Performance: The quality of the TE decision. It is presented by the Normalized MLU, defined as the ratio of the MLU achieved by the ML-driven TE scheme to that of the optimal solution (obtained using the Gurobi optimization solver). (ii) Memory Usage: The GPU memory consumption during training. (iii) Time-to-Performance: The training time required to achieve specific performance targets (measured in Normalized MLU thresholds), which indicates the convergence speed of the method.

**baselines.** We compare Geminet with state-of-the-art ML-based TE schemes, including HARP, DOTE, TEAL, RedTE, and FIGRET. HARP, DOTE, TEAL, and RedTE are described in §2.1. FIGRET, designed for traffic uncertainty, shares DOTE’s architecture but introduces a new loss function to enhance robustness. When evaluated with an accurate traffic matrix, FIGRET reduces to DOTE, as both use the exact matrix as input. Under traffic uncertainty (§5.6), both use historical traffic matrices as input, enabling FIGRET’s robustness mechanism. Additionally, RedTE determines splitting ratios using local information from the previous time step, so it is only evaluated under traffic uncertainty (§5.6). Hyperparameter details are provided in Appendix C.6.

## 5.2 Handling topology changes

We compare the performance of Geminet with HARP on the changing topology DynGeant. The results are summarized in Table 2. From these results, we make two key observations:

- Under the premise that Geminet and HARP perform similarly, the memory usage of Geminet is 4% that of HARP.

Regarding convergence speed, Geminet reaches the target performance 1.9×, 2.7×, and 3.6× faster at the 1.2, 1.18, and 1.16 Normalized MLU thresholds, respectively.

- For HARP, memory consumption for handling similar-scale topologies, GEANT and DynGeant, is 0.07 and 0.53, respectively. This is because HARP first applies a graph neural network to generate edge embeddings and then uses a transformer to derive path embeddings. In static topologies, where the network structure and edge-path mappings remain unchanged, embeddings are computed only once. However, in changing topologies, HARP must recompute embeddings for each data point.

		Geminet	HARP
Performance (Normalized MLU)	Average	1.12	1.14
	25th Pct.	1.07	1.09
	50th Pct.	1.12	1.11
	75th Pct.	1.16	1.16
	99th Pct.	1.28	1.33
Memory Usage (GiB)		<b>0.02</b>	0.53
Time-to-Performance (s) (1.2/1.18/1.16 Normalized MLU)		<b>43/53/59</b>	82/146/214

**Table 2: Comparing Geminet and HARP on DynGeant.**

## 5.3 Comparing in one-cluster topologies

We compare Geminet, HARP, DOTE/FIGRET, and TEAL on one-cluster topologies, focusing on performance, neural network parameters, GPU memory usage, and convergence speed.

**Performance.** Figure 4(a) and Figure 4(b) summarize TE performance for two scenarios: (a) when tunnel orders in training and testing are the same, and (b) when they are shuffled. Geminet and HARP perform well in both cases, while DOTE struggles under shuffled conditions. As discussed in §2.1, Teal’s independent optimization for each source-destination pair may sometimes lead to suboptimal results, e.g., as shown in Figure 4(a). Results for additional topologies are provided in Appendix D.4, which exhibit similar characteristics.

**Number of neural network model parameters.** In Figure 5(a), we analyze how the number of neural network model parameters for Geminet, HARP, TEAL, and DOTE/FIGRET change with topology size. It can be observed that the number of Geminet’s model parameters is significantly smaller than the other three methods. For example, on the GEANT topology, the number of parameters in Geminet is only 0.07 of TEAL, 0.026 of HARP, and  $4 \times 10^{-4}$  of DOTE/FIGRET. Smaller parameter sizes offer many advantages: in addition to requiring less model memory, smaller models typically require less training data, are less prone to overfitting, and may exhibit better generalization performance [46].

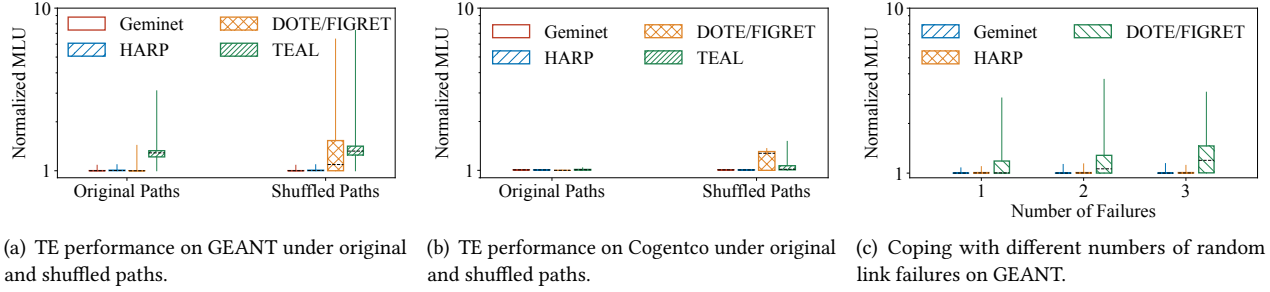


**Figure 4: TE performance across different scenarios, including path shuffling (4(a), 4(b)) and link failures (4(c)).**

**Memory Usage.** The GPU memory usage results are summarized in Table 1. As shown, Geminet has the smallest memory usage among all schemes. Moreover, compared to HARP, another TE scheme capable of handling changing topologies, Geminet significantly reduces memory usage. For instance, on the small-scale GEANT topology, its memory usage is only 25.6% of HARP, and on the large-scale Meta WEB DC ToR topology, its memory usage is just 9.3% of HARP. For HARP, on the KDL topology, it is unable to run even on modern GPUs with 80 GiB of memory. According to our evaluations, even when the batch size is set to 1 and float16 precision is used for training, HARP still consumes 67 GiB of memory on the KDL topology.

DOTE, and HARP to reach a normalized MLU of 1.01 are 249s, 243s, and 1357s, respectively. The convergence speed of Geminet is 5.45× faster than that of HARP.

### 5.4 Handling link failure

In this section, we compare the ability of ML-based TE schemes to handle link failures. Since TEAL sometimes performs sub-optimally, as evaluated in §5.4, we focus only on comparing Geminet, HARP, and DOTE. For Geminet and HARP, handling link failures can be regarded as a change in edge capacity. DOTE’s strategy for handling link failures is local rescaling [37]. Specifically, for any flow, traffic on unavailable tunnels is rerouted to the surviving tunnels in proportion to the split ratios in the absence of link failure.

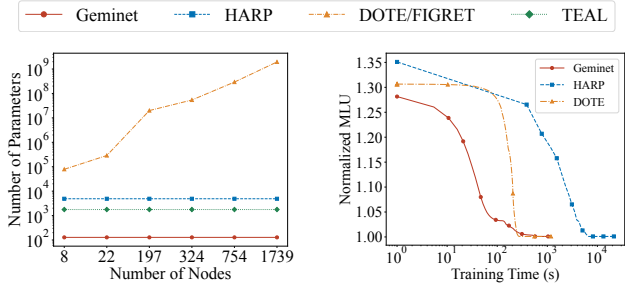
Figure 4(c) shows the impact of randomly selected link failures in the GEANT. Geminet performs on par with HARP in handling link failures. Moreover, ML-based TE schemes like Geminet and HARP, which support variable topologies, outperform DOTE, which relies on rerouting. Results for other topologies in Appendix D.7 exhibit similar trends.

### 5.5 Training on sub-traffic matrices

We evaluate the effectiveness of the strategy proposed in §4.4 on two large-scale topologies, Meta WEB ToR-level and KDL. In this evaluation, we test different numbers of partitions: 2, 4, and 8, to evaluate performance and GPU memory.

**Memory usage.** Figure 6 shows the GPU memory consumption during training. As the number of partitions increases, peak memory usage decreases significantly. For example, on the KDL dataset, using two partitions reduces GPU memory usage to 49.8% of the non-partitioned baseline, while four partitions further reduce it to 24.4%.

**Performance.** We evaluate the performance of our partition-based training strategy by considering two approaches: training with only one partitioned group, and training with all groups. As shown in Figure 7, even when training with only a single group, Geminet’s performance remains robust, with minimal degradation. Specifically, on the ToR WEB dataset,



(a) Comparison of the number of model parameters. (b) Comparison of Time-to-Performance on KDL.

**Figure 5: Comparison of the number of model parameters and Time-to-Performance across different TE schemes.**

**Time-to-Performance.** We compare Time-to-Performance of several methods on large-scale KDL topologies, as shown in Figure 5(b). Due to the out-of-memory issue with HARP, its batch size is set to 1. Considering that Teal may be sub-optimal, we do not include it in the statistics. As illustrated in Figure 5(b), Geminet converges faster than HARP and performs comparably to DOTE, which only uses a few fully connected layers. Specifically, the times required for Geminet,

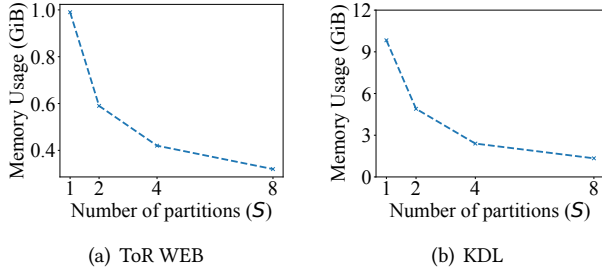


**Figure 6: Changes in GPU memory usage with the number of partitions (S).**

the performance drops are 0.7%, 0.1%, and 0.09% for  $S = 2$ ,  $S = 4$ , and  $S = 8$ , respectively; for the KDL dataset, the corresponding drops are 0.4%, 0.7%, and 0.05%. This stability can be attributed to three key factors: (1) our method learns the iterative adjustment process, which is largely independent of the specific traffic demand patterns; (2) we partition only the source-destination pairs rather than the topology itself, so while absolute edge loads may vary, the adjustment of  $\lambda$  mainly depends on edges with higher relative loads (those close to MLU), making the impact of absolute edge loads less significant during training; and (3) Geminet employs a neural network with relatively few parameters, which enhances generalization [46]. Results for training with all groups are provided in Appendix D.6, where we show that using all groups achieves performance comparable to the non-partitioned baseline.

## 5.6 Handling traffic uncertainty

**Performance comparison across TE schemes.** Our results so far have evaluated schemes using exact traffic matrices. However, in practice, both optimization solvers and ML-based schemes operate with predicted traffic matrices. Consequently, we next aim to evaluate the performance of our algorithm under traffic uncertainty.

Similar to HARP [7], we first predict the traffic matrices and then feed these predicted matrices to Geminet. During the training phase, TE configurations are generated using the predicted matrix, but the loss is computed using the actual matrix. In the inference phase, only the predicted matrix is available to Geminet. For traffic prediction, we employ two methods, as described in [7]: (i) MovAvg: The predicted value is the average of the corresponding historical window. (ii) LinReg: The predicted value is based on linear regression applied to the historical window. The historical window length is set to 12 [7, 37].

The performance comparison of Geminet, HARP, and Gurobi on the dynamic topology DynGeant under predicted traffic demands is summarized in Figure 8. First, similar to

findings in [7], ML-based TE demonstrates an ability to learn robustness against prediction errors compared to Gurobi. Second, Geminet shows a lower mean and 50th percentile compared to HARP. However, in extreme cases, such as the top end of the whiskers in the MovAvg boxplot, Geminet exhibits higher values. This is due to their differing adjustment strategies: Geminet adjusts at the edge level, while HARP operates at the path level. Edge-level adjustments aggregate flows from multiple paths, allowing prediction errors to partially cancel out, which generally benefits Geminet. However, when prediction errors across paths align, this cancellation effect diminishes, leading to greater errors and causing Geminet to underperform in extreme cases.

To compare Geminet and HARP with end-to-end approaches like DOTE and FIGRET, which directly map historical traffic matrices to next-time TE decisions, we evaluate them on the WEB DC topology under two scenarios: (i) fixed edge capacities and (ii) changing edge capacities, with FIGRET’s traffic burst handling weight set to 0.1. The results, summarized in Figure 9, show that end-to-end methods outperform Geminet and HARP in handling traffic uncertainty when edge capacities are fixed. However, their performance degrades significantly when edge capacities change (PoD WEB CC), as they assume a static topology.

**Excessive memory overhead in RedTE.** We report the memory usage of all TE schemes except RedTE in Table 1. RedTE’s memory usage exceeds 80 GiB on all topologies except GEANT. Therefore, we analyze its model memory usage theoretically, based on its open-source code [1], to illustrate the root cause. The critic network in RedTE takes two inputs: the splitting ratios for all source-destination pairs and the aggregated local environment of all nodes. On the KDL topology, with 4 paths per source-destination pair, the input sizes are 2,271,048 and 569,552, respectively. According to the open-source implementation, each critic contains 219 million parameters. Using float32, storing all critic models during training requires approximately 613 GB of memory, highlighting RedTE’s poor scalability.

## 5.7 Computation Time

In this section, we analyze the computation time of ML-based TE schemes and Gurobi. During the evaluation, we create the model and run inference directly for ML-based TE schemes with too large memory requirements to train, as whether the model has been trained does not affect inference time. The results are summarized in Figure 10. From the results, we draw the following findings: (i) ML-based TE schemes have a significant advantage over Gurobi in computation time, being faster than two orders of magnitude for large-scale topologies such as WEB ToR and KDL. (ii) The two TE schemes, Geminet and HARP, which are capable of handling

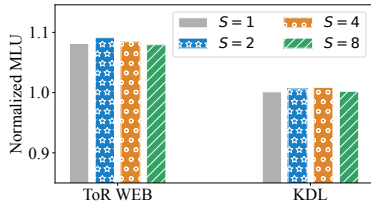


Figure 7: Changes in average normalized MLU with the number of partitions ( $S$ ) when training with just one of the partitioned groups.

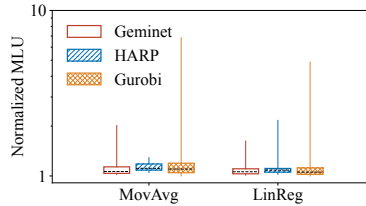


Figure 8: Comparison of Geminet, HARP, and Gurobi performance on DynGeant with predicted traffic demands from various predictors.

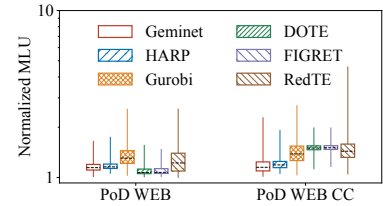


Figure 9: Comparison of TE schemes on PoD WEB under traffic uncertainty, where PoD WEB CC represents changing edge capacity.

changing topologies, require iterative adjustments, making them slower than TEAL and DOTE. (iii) Among the ML-based TE schemes designed for changing topologies, Geminet is faster than HARP. On the KDL topology, Geminet achieves a computation speed 2.3× that of HARP. (iv) For ASN, its average path length is shorter than KDL, resulting in a sparser path-to-edge mapping. Thus, the computation time does not increase significantly for TEAL, Geminet, and HARP, which all process path-edge relationships during inference. In contrast, computation time increases on ASN for DOTE, whose model size depends only on the number of nodes.

### 5.8 Fewer parameters, less training data

In this section, we compare Geminet, a TE scheme with fewer parameters, to DOTE, which has significantly more parameters, under reduced training data conditions to highlight the advantage of models with fewer parameters requiring less data to train effectively. The results, summarized in Figure 11, illustrate the relationship between model quality and training data quantity for Geminet and DOTE. As shown in Figure 11, Geminet requires much less training data than DOTE due to its smaller number of parameters—only 20% of the data is sufficient. This lightweight architecture makes Geminet more practical for real-world deployment.

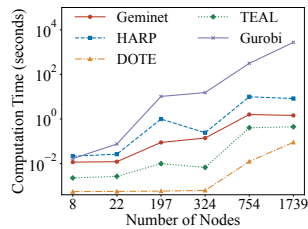


Figure 10: Comparison of computation times across different topology sizes.

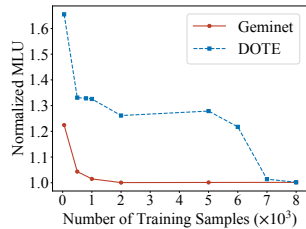


Figure 11: Relationship between model quality and data quantity on GEANT.

### 5.9 Visualizing Geminet’s iterative process

To better understand how Geminet solves the optimization problem through iterative adjustment, we visualize its internal optimization trajectory. This not only enhances interpretability but also empirically verifies that the iterative nature of gradient descent can be learned and that Geminet successfully captures this behavior. The results are shown in Figure 12. For each topology, we use the first case from the test set for illustration. Specifically, we compute the cosine similarity between the  $\lambda$ -values produced by Geminet at each iteration and the optimal  $\lambda$  obtained by solving the problem with Gurobi. We observe that, over time, the relative pattern of  $\lambda$  produced by Geminet becomes increasingly similar to that of the optimal solution. It is worth noting that the final  $\lambda$  values produced by Geminet do not exactly match the optimal ones. This is expected: under the complementary slackness condition in Equation (8), only edges with utilization equal to the maximum have non-zero  $\lambda$  in the Gurobi solution, while all others are zero. In contrast, during training, Geminet reconstructs  $r_p$  using a softmin from  $\sum_{e \in p} \lambda$ , making the relative magnitudes of  $\lambda$  important. Bottleneck edges tend to have larger  $\lambda$  values, while others have smaller—but not necessarily zero values. Therefore, we normalize the cosine similarity to account for this difference.

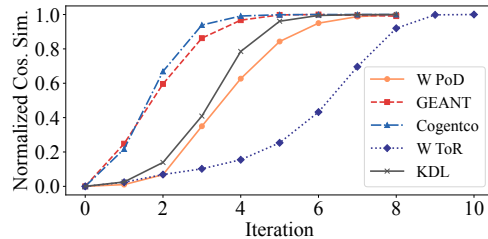


Figure 12: Cosine similarity between Geminet’s  $\lambda$  and the optimal  $\lambda$  over iterations.

## 6 DISCUSSION

**Potential of integrating prediction tasks into Geminet for handling traffic uncertainty.** Figure 9 in §5.6 shows that in static topologies, end-to-end approaches like DOTE/-FIGRET, which integrate prediction tasks with optimization by directly mapping historical traffic matrices to TE decisions, outperform two-stage methods like Geminet and HARP, which separate prediction and optimization, in handling traffic uncertainty. This highlights the effectiveness of integrating prediction tasks with optimization. The key advantage lies in addressing the mismatch between prediction metrics (e.g., MSE) and optimization objectives (e.g., MLU). Prediction alone cannot account for the impact of topology, whereas integration eliminates this limitation [37]. Incorporating this idea into TE schemes that can handle changing topologies has the potential to enhance their ability to handle traffic uncertainty. However, this integration is not as simple as replacing their input with historical traffic matrices, as their iterative processes rely on precise traffic demands to compute MLU. How to achieve this remains an open challenge, which we will explore in future work.

**Improving Geminet’s solution time.** As discussed in §5.7, Geminet takes longer to compute solutions than DOTE, primarily because DOTE produces results directly through a few fully connected layers, whereas Geminet relies on an iterative adjustment process. This process requires computing gradient-related quantities, such as MLU, using Equation (20), which involves sparse matrix multiplications. These computations create a bottleneck in Geminet’s solution time. This is the cost of supporting changing topologies, which remains an area for future optimization.

**Extensibility to other objectives.** Other optimization objectives can generally be categorized into two types. The first includes convex objectives, such as maximizing total throughput, which can often be formulated similarly to MLU. Geminet can be adapted to optimize these objectives with only minor modifications. The second category consists of non-convex and non-differentiable objectives, such as minimizing flow completion time or packet loss rate, which often lack explicit analytical formulations. These present a greater challenge for existing ML-based approaches, which are currently not well suited to handle such objectives. A potential solution is to integrate a simulator that can approximate these objectives and provide feedback, allowing an ML-based method to iteratively refine its strategy. We leave this exploration for future work.

## 7 RELATED WORK

TE is widely used in WANs and data centers. However, as network topologies expand, TE optimization becomes increasingly complex and time-consuming. To address this,

efforts have focused on accelerating TE, including scaling optimization via decomposition methods [2, 20, 24, 36]. However, these methods are constrained by limited subproblem partitioning, balancing runtime and TE performance but achieving only modest parallelism and speedup. This has driven interest in ML-based TE as an alternative.

ML-based TE has been extensively studied [7, 21, 33–35, 37, 48, 51, 52]. TEAL [52] leverages ML to accelerate TE decision-making, while DOTE [37] optimizes routing under traffic uncertainty using historical traffic demand. FIGRET [34] enhances robustness against traffic bursts by incorporating an additional loss function. Then, HARP [7] introduces ML-based TE for topology variations, but its high computational cost limits practicality. In this work, we propose a lightweight ML-based TE solution for dynamic topologies, making it more suitable for real-world deployment.

For link failures, TE schemes adopt either proactive or reactive strategies. Proactive methods ensure congestion-free operation across all predefined failure scenarios [25, 32, 50] or sufficient scenarios to meet a desired percentile target [11, 15], often by conservatively allocating bandwidth. Reactive methods respond post-failure via local rescaling, which adjusts existing allocations, or explicit recomputation [2, 31], which recalculates routes. Proactive and reactive approaches can be combined to enhance network resilience. When handling link failures, our approach is a reactive method that dynamically adapts to post-failure topologies.

## 8 CONCLUSION

In this work, we introduce Geminet, a framework that leverages the duality-based iterative process for lightweight traffic engineering in changing topologies. Geminet decouples the neural network from topology information by learning the gradient descent process and employs duality theory to transform the optimization problem from path-level to edge-level. Our evaluation results demonstrate that Geminet significantly reduces computational and memory overhead without sacrificing performance, showing its potential for deployment in production environments.

## REFERENCES

- [1] 2024. GitHub repository containing the RedTE code. <https://github.com/NASP-THU/RedTE.git>. (2024).
- [2] Firas Abuzaid, Srikanth Kandula, Behnaz Arzani, Ishai Menache, Matei Zaharia, and Peter Bailis. 2021. Contracting wide-area network topologies to solve flow problems quickly. In *18th USENIX Symposium on Networked Systems Design and Implementation (NSDI 21)*. 175–200.
- [3] Sugam Agarwal, Murali Kodialam, and TV Lakshman. 2013. Traffic engineering in software defined networks. In *2013 Proceedings IEEE INFOCOM*. IEEE, 2211–2219.
- [4] Ian F Akyildiz, Ahyoung Lee, Pu Wang, Min Luo, and Wu Chou. 2014. A roadmap for traffic engineering in SDN-OpenFlow networks. *Computer Networks* 71 (2014), 1–30.

- [5] Mohammad Al-Fares, Sivasankar Radhakrishnan, Barath Raghavan, Nelson Huang, Amin Vahdat, et al. 2010. Hedera: dynamic flow scheduling for data center networks.. In *Nsdi*, Vol. 10. San Jose, USA, 89–92.
- [6] Mohammad Alizadeh, Tom Edsall, Sarang Dharmapurikar, Ramanan Vaidyanathan, Kevin Chu, Andy Fingerhut, Vinh The Lam, Francis Matus, Rong Pan, Navindra Yadav, et al. 2014. CONGA: Distributed congestion-aware load balancing for datacenters. In *Proceedings of the 2014 ACM conference on SIGCOMM*. 503–514.
- [7] Abd AlRhaman AlQiam, Yuanjun Yao, Zhaodong Wang, Satyajeet Singh Ahuja, Ying Zhang, Sanjay G Rao, Bruno Ribeiro, and Mohit Tawarmalani. 2024. Transferable Neural WAN TE for Changing Topologies. In *Proceedings of the ACM SIGCOMM 2024 Conference*. 86–102.
- [8] David Applegate and Edith Cohen. 2003. Making intra-domain routing robust to changing and uncertain traffic demands: Understanding fundamental tradeoffs. In *Proceedings of the 2003 conference on Applications, technologies, architectures, and protocols for computer communications*. 313–324.
- [9] Yossi Azar, Edith Cohen, Amos Fiat, Haim Kaplan, and Harald Racke. 2003. Optimal oblivious routing in polynomial time. In *Proceedings of the thirty-fifth annual ACM symposium on Theory of computing*. 383–388.
- [10] Theophilus Benson, Ashok Anand, Aditya Akella, and Ming Zhang. 2011. MicroTE: Fine grained traffic engineering for data centers. In *Proceedings of the seventh conference on emerging networking experiments and technologies*. 1–12.
- [11] Jeremy Bogle, Nikhil Bhatia, Manya Ghobadi, Ishai Menache, Nikolaj Björner, Asaf Valadarsky, and Michael Schapira. 2019. TEAVAR: striking the right utilization-availability balance in WAN traffic engineering. In *Proceedings of the ACM Special Interest Group on Data Communication*. 29–43.
- [12] Stephen Boyd and Lieven Vandenbergh. 2004. *Convex optimization*. Cambridge university press.
- [13] CAIDA. 2022. The CAIDA AS Relationships Dataset. (2022).
- [14] Peirui Cao, Shizhen Zhao, Min Yee The, Yunzhuo Liu, and Xinbing Wang. 2021. TROD: Evolving from electrical data center to optical data center. In *2021 IEEE 29th International Conference on Network Protocols (ICNP)*. IEEE, 1–11.
- [15] Yiyang Chang, Chuan Jiang, Ashish Chandra, Sanjay Rao, and Mohit Tawarmalani. 2019. Lancet: Better network resilience by designing for pruned failure sets. *Proceedings of the ACM on Measurement and Analysis of Computing Systems* 3, 3 (2019), 1–26.
- [16] Li Chen, Justinas Lingys, Kai Chen, and Feng Liu. 2018. Auto: Scaling deep reinforcement learning for datacenter-scale automatic traffic optimization. In *Proceedings of the 2018 conference of the ACM special interest group on data communication*. 191–205.
- [17] Marco Chiesa, Gábor Rétvári, and Michael Schapira. 2016. Lying your way to better traffic engineering. In *Proceedings of the 12th International on Conference on emerging Networking EXperiments and Technologies*. 391–398.
- [18] Anwar Elwalid, Cheng Jin, Steven Low, and Indra Widjaja. 2001. MATE: MPLS adaptive traffic engineering. In *Proceedings IEEE INFOCOM 2001. Conference on Computer Communications. Twentieth Annual Joint Conference of the IEEE Computer and Communications Society (Cat. No. 01CH37213)*, Vol. 3. IEEE, 1300–1309.
- [19] Bernard Fortz and Mikkel Thorup. 2000. Internet traffic engineering by optimizing OSPF weights. In *Proceedings IEEE INFOCOM 2000. conference on computer communications. Nineteenth annual joint conference of the IEEE computer and communications societies (Cat. No. 00CH37064)*, Vol. 2. IEEE, 519–528.
- [20] Amitabha Ghosh, Sangtae Ha, Edward Crabbe, and Jennifer Rexford. 2013. Scalable multi-class traffic management in data center backbone networks. *IEEE Journal on Selected Areas in Communications* 31, 12 (2013), 2673–2684.
- [21] Fei Gui, Songtao Wang, Dan Li, Li Chen, Kaihui Gao, Congcong Min, and Yi Wang. 2024. RedTE: Mitigating subsecond traffic bursts with real-time and distributed traffic engineering. In *Proceedings of the ACM SIGCOMM 2024 Conference*. 71–85.
- [22] Chi-Yao Hong, Srikanth Kandula, Ratul Mahajan, Ming Zhang, Vijay Gill, Mohan Nanduri, and Roger Wattenhofer. 2013. Achieving high utilization with software-driven WAN. In *Proceedings of the ACM SIGCOMM 2013 Conference on SIGCOMM*. 15–26.
- [23] Sushant Jain, Alok Kumar, Subhasree Mandal, Joon Ong, Leon Poutievski, Arjun Singh, Subbaiah Venkata, Jim Wanderer, Junlan Zhou, Min Zhu, et al. 2013. B4: Experience with a globally-deployed software defined WAN. *ACM SIGCOMM Computer Communication Review* 43, 4 (2013), 3–14.
- [24] Chuan Jiang, Zixuan Li, Sanjay Rao, and Mohit Tawarmalani. 2022. Flexile: Meeting bandwidth objectives almost always. In *Proceedings of the 18th International Conference on emerging Networking EXperiments and Technologies*. 110–125.
- [25] Chuan Jiang, Sanjay Rao, and Mohit Tawarmalani. 2020. PCF: provably resilient flexible routing. In *Proceedings of the Annual conference of the ACM Special Interest Group on Data Communication on the applications, technologies, architectures, and protocols for computer communication*. 139–153.
- [26] Wenjie Jiang, Rui Zhang-Shen, Jennifer Rexford, and Mung Chiang. 2009. Cooperative content distribution and traffic engineering in an ISP network. In *Proceedings of the eleventh international joint conference on Measurement and modeling of computer systems*. 239–250.
- [27] Srikanth Kandula, Dina Katabi, Bruce Davie, and Anna Charny. 2005. Walking the tightrope: Responsive yet stable traffic engineering. *ACM SIGCOMM Computer Communication Review* 35, 4 (2005), 253–264.
- [28] Srikanth Kandula, Ishai Menache, Roy Schwartz, and Spandana Raj Babbula. 2014. Calendaring for wide area networks. In *Proceedings of the 2014 ACM conference on SIGCOMM*. 515–526.
- [29] Simon Knight, Hung X Nguyen, Nickolas Falkner, Rhys Bowden, and Matthew Roughan. 2011. The internet topology zoo. *IEEE Journal on Selected Areas in Communications* 29, 9 (2011), 1765–1775.
- [30] Alok Kumar, Sushant Jain, Uday Naik, Anand Raghuraman, Nikhil Kasinadhuni, Enrique Cauich Zermeno, C Stephen Gunn, Jing Ai, Björn Carlin, Mihai Amarandei-Stavila, et al. 2015. BwE: Flexible, hierarchical bandwidth allocation for WAN distributed computing. In *Proceedings of the 2015 ACM Conference on Special Interest Group on Data Communication*. 1–14.
- [31] Praveen Kumar, Yang Yuan, Chris Yu, Nate Foster, Robert Kleinberg, Petr Lapukhov, Chiun Lin Lim, and Robert Soulé. 2018. {Semi-oblivious} traffic engineering: The road not taken. In *15th USENIX Symposium on Networked Systems Design and Implementation (NSDI 18)*. 157–170.
- [32] Hongqiang Harry Liu, Srikanth Kandula, Ratul Mahajan, Ming Zhang, and David Gelernter. 2014. Traffic engineering with forward fault correction. In *Proceedings of the 2014 ACM Conference on SIGCOMM*. 527–538.
- [33] Libin Liu, Li Chen, Hong Xu, and Hua Shao. 2020. Automated traffic engineering in SDWAN: Beyond reinforcement learning. In *IEEE INFOCOM 2020-IEEE Conference on Computer Communications Workshops (INFOCOM WKSHPS)*. IEEE, 430–435.
- [34] Ximeng Liu, Shizhen Zhao, Yong Cui, and Xinbing Wang. 2024. FIGRET: Fine-Grained Robustness-Enhanced Traffic Engineering. In *Proceedings of the ACM SIGCOMM 2024 Conference*. 117–135.
- [35] Bashir Mohammed, Mariam Kiran, and Nandini Krishnaswamy. 2019. DeepRoute on Chameleon: Experimenting with large-scale reinforcement learning and SDN on Chameleon testbed. In *2019 IEEE 27th International Conference on Network Protocols (ICNP)*. IEEE, 1–2.

- [36] Deepak Narayanan, Fiodar Kazhamiaka, Firas Abuzaid, Peter Kraft, Akshay Agrawal, Srikanth Kandula, Stephen Boyd, and Matei Zaharia. 2021. Solving large-scale granular resource allocation problems efficiently with pop. In *Proceedings of the ACM SIGOPS 28th Symposium on Operating Systems Principles*. 521–537.
- [37] Yarin Perry, Felipe Vieira Frujeri, Chaim Hoch, Srikanth Kandula, Ishai Menache, Michael Schapira, and Aviv Tamar. 2023. {DOTE}: Rethinking (Predictive){WAN} Traffic Engineering. In *20th USENIX Symposium on Networked Systems Design and Implementation (NSDI 23)*. 1557–1581.
- [38] Leon Poutievski, Omid Mashayekhi, Joon Ong, Arjun Singh, Mukarram Tariq, Rui Wang, Jianan Zhang, Virginia Beaugard, Patrick Conner, Steve Gribble, et al. 2022. Jupiter evolving: transforming google’s datacenter network via optical circuit switches and software-defined networking. In *Proceedings of the ACM SIGCOMM 2022 Conference*. 66–85.
- [39] Matthew Roughan, Albert Greenberg, Charles Kalmanek, Michael Rumsewicz, Jennifer Yates, and Yin Zhang. 2002. Experience in measuring backbone traffic variability: Models, metrics, measurements and meaning. In *Proceedings of the 2nd ACM SIGCOMM Workshop on Internet Measurement*. 91–92.
- [40] Matthew Roughan, Mikkel Thorup, and Yin Zhang. 2003. Traffic engineering with estimated traffic matrices. In *Proceedings of the 3rd ACM SIGCOMM Conference on Internet Measurement*. 248–258.
- [41] Arjun Roy, Hongyi Zeng, Jasmeet Bagga, George Porter, and Alex C Snoeren. 2015. Inside the social network’s (datacenter) network. In *Proceedings of the 2015 ACM Conference on Special Interest Group on Data Communication*. 123–137.
- [42] Mohammad Shoeybi, Mostofa Patwary, Raul Puri, Patrick LeGresley, Jared Casper, and Bryan Catanzaro. 2019. Megatron-lm: Training multi-billion parameter language models using model parallelism. *arXiv preprint arXiv:1909.08053* (2019).
- [43] Nimit S Sohoni, Christopher R Aberger, Megan Leszczynski, Jian Zhang, and Christopher Ré. 2019. Low-memory neural network training: A technical report. *arXiv preprint arXiv:1904.10631* (2019).
- [44] Martin Suchara, Dahai Xu, Robert Doverspike, David Johnson, and Jennifer Rexford. 2011. Network architecture for joint failure recovery and traffic engineering. *ACM SIGMETRICS Performance Evaluation Review* 39, 1 (2011), 97–108.
- [45] Min Yee Teh, Shizhen Zhao, Peirui Cao, and Keren Bergman. 2020. COUDER: robust topology engineering for optical circuit switched data center networks. *arXiv preprint arXiv:2010.00090* (2020).
- [46] Yingjie Tian and Yuqi Zhang. 2022. A comprehensive survey on regularization strategies in machine learning. *Information Fusion* 80 (2022), 146–166.
- [47] Steve Uhlig, Bruno Quoitin, Jean Lepropre, and Simon Balon. 2006. Providing public intradomain traffic matrices to the research community. *ACM SIGCOMM Computer Communication Review* 36, 1 (2006), 83–86.
- [48] Asaf Valadarsky, Michael Schapira, Dafna Shahaf, and Aviv Tamar. 2017. Learning to route. In *Proceedings of the 16th ACM workshop on hot topics in networks*. 185–191.
- [49] Hao Wang, Haiyong Xie, Lili Qiu, Yang Richard Yang, Yin Zhang, and Albert Greenberg. 2006. COPE: Traffic engineering in dynamic networks. In *Proceedings of the 2006 conference on Applications, technologies, architectures, and protocols for computer communications*. 99–110.
- [50] Ye Wang, Hao Wang, Ajay Mahimkar, Richard Alimi, Yin Zhang, Lili Qiu, and Yang Richard Yang. 2010. R3: resilient routing reconfiguration. In *Proceedings of the ACM SIGCOMM 2010 conference*. 291–302.
- [51] Zhiyuan Xu, Jian Tang, Jingsong Meng, Weiyi Zhang, Yanzhi Wang, Chi Harold Liu, and Dejun Yang. 2018. Experience-driven networking: A deep reinforcement learning based approach. In *IEEE INFOCOM 2018-IEEE conference on computer communications*. IEEE, 1871–1879.
- [52] Zhiying Xu, Francis Y Yan, Rachee Singh, Justin T Chiu, Alexander M Rush, and Minlan Yu. 2023. Teal: Learning-accelerated optimization of wan traffic engineering. In *Proceedings of the ACM SIGCOMM 2023 Conference*. 378–393.
- [53] Nicu Florin Zaicu, Matthew Luckie, Richard Nelson, and Marinho Barcellos. 2021. Helix: Traffic Engineering for Multi-Controller SDN. In *Proceedings of the ACM SIGCOMM Symposium on SDN Research (SOSR)*. 80–87.
- [54] Zhizhen Zhong, Manya Ghobadi, Alaa Khaddaj, Jonathan Leach, Yiting Xia, and Ying Zhang. 2021. ARROW: restoration-aware traffic engineering. In *Proceedings of the 2021 ACM SIGCOMM 2021 Conference*. 560–579.

## APPENDIX

### A NOTATION TABLE

We tabulate the notations in Table 3.

Notation	Description
$G(V, E, c)$	Network topology, $V$ is node set, $E$ is edge set, and $c$ assigns capacities to edges
$D$	Demand matrix, where $D_{ij}$ denotes the traffic from $i$ to $j$
$P$	Network paths, where $P_{st}$ denotes the set of network paths through which the source $s$ communicates with destination $t$
$r_p$	The split ratio of the traffic demand from $s$ to $t$ forwarded along path $p$
$\mathcal{R}$	TE configuration
$m$	Max Link Utilization
$U(e)$	Link utilization of edge $e$
$\lambda_e$	Lagrange dual variable associated with edge $e$
$L(\mathcal{R}, m, \lambda)$	Lagrangian function
$\Phi$	The set of all paths
$\xi^{( \Phi ,  E )}$	Path-to-Edge Matrix: A binary matrix indicating whether a given path $i$ contains edge $j$ . Specifically, $\xi_{ij} = 1$ if edge $j$ is part of path $i$
$\Psi^{( \Phi , 1)}$	A vector representing the potential load associated with each path
$\Omega$	The set of all source-destination pairs
$S$	The number of sub-traffic matrices obtained by partitioning the traffic matrix.

Table 3: Notations used in this paper.

## B MATHEMATICAL PRELIMINARIES

### B.1 Summation order exchange detail

We explain the transition from the second to the third line in Equation (4). We begin by writing out the second term of the second line in Equation (4), which is given by:

$$\sum_{e \in E} \sum_{s, t \in V} \sum_{p \in P_{st}, p \ni e} \lambda_e D_{st} r_p. \quad (10)$$

To facilitate this transition, we introduce the indicator function  $I(p, e)$ , which equals 1 if path  $p$  includes edge  $e$  (denoted  $p \ni e$ ), and 0 otherwise. Incorporating  $I(p, e)$  into the Equation (10), we rewrite it as:

$$\sum_{e \in E} \sum_{s, t \in V} \sum_{p \in P_{st}} I(p, e) \lambda_e D_{st} r_p. \quad (11)$$

Since the summations in Equation (11) are independent and do not interfere with each other, we can rearrange the order

of summation as follows:

$$\sum_{s, t \in V} \sum_{p \in P_{st}} \sum_{e \in E} I(p, e) \lambda_e D_{st} r_p. \quad (12)$$

Given that the indicator function  $I(p, e)$  equals 1 only when  $p \ni e$ , the summation  $\sum_{e \in E} I(p, e)$  simplifies to  $\sum_{e \in p}$ . Consequently, Equation (12) can be rewritten as:

$$\sum_{s, t \in V} \sum_{p \in P_{st}} \sum_{e \in p} \lambda_e D_{st} r_p, \quad (13)$$

which is the second term of the third line in Equation (4).

### B.2 KKT condition

In this section, we first introduce the concept of *Karush-Kuhn-Tucker* (KKT) conditions. Consider the optimization problem in the standard form:

$$\begin{array}{ll} \text{minimize} & f_0(x) \\ \text{subject to} & f_i(x) \leq 0, \quad i = 1, \dots, m, \\ & h_i(x) = 0, \quad i = 1, \dots, p. \end{array} \quad (14)$$

We define the Lagrangian  $L$  associated with the problem (14) as

$$L(x, \lambda, \nu) = f_0(x) + \sum_{i=1}^m \lambda_i f_i(x) + \sum_{i=1}^p \nu_i h_i(x), \quad (15)$$

where  $\lambda_i$  denotes the Lagrange multiplier associated with the  $i$ th inequality constraint  $f_i(x) \leq 0$ , and  $\nu_i$  as the Lagrange multiplier associated with the  $i$ th equality constraint  $h_i(x) = 0$ .

In order to determine the conditions under which a solution to this optimization problem can be considered optimal, a classic set of requirements known as the KKT conditions comes into play. We present these conditions in the following lemma:

LEMMA 1. *For any optimization problem with differentiable objective and constraint functions for which strong duality obtains, any pair of primal and dual optimal points must satisfy the KKT conditions [12]:*

$$\begin{array}{ll} f_i(x^*) \leq 0, & i = 1, \dots, m, \\ h_i(x^*) = 0, & i = 1, \dots, p, \\ \lambda_i^* \geq 0, & i = 1, \dots, m, \\ \lambda_i^* f_i(x^*) = 0, & i = 1, \dots, m, \end{array} \quad (16)$$

$$\nabla f_0(x^*) + \sum_{i=1}^m \lambda_i^* \nabla f_i(x^*) + \sum_{i=1}^p \nu_i^* \nabla h_i(x^*) = 0.$$

### B.3 Primal optimal from Lagrangian

LEMMA 2. *The solution of the Equation (5) is primal optimal.*

To proof LEMMA 2, we begin by presenting two foundational lemmas from duality theory [12]:

LEMMA 3. *For linear programming problems, strong duality always holds if the primal problem is feasible and bounded [12].*

LEMMA 4. *If strong duality holds and the optimal dual variables  $\lambda^*$ ,  $v^*$  are known, and the minimizer of  $L(x, \lambda^*, v^*)$ , i.e., the solution of*

$$\text{minimize } f_0(x) + \sum_{i=1}^m \lambda_i^* f_i(x) + \sum_{i=1}^p v_i^* h_i(x), \quad (17)$$

*is unique. Then if the solution of Equation 17 is primal feasible, it must be primal optimal [12].*

Given LEMMA 3 and LEMMA 4, we proof LEMMA 2 as follow:

PROOF. Given that the original problem specified by Equation (1) is a linear programming problem, we apply LEMMA 3 to assert that strong duality holds. Furthermore, the minimization of the Lagrangian, as formulated in Equation (5), constitutes another linear problem. Since linear problems are a subset of convex optimization problems, the solution is unique. Therefore, according to LEMMA 4, solving Equation (5) yields the optimal solution to the original problem.  $\square$

### B.4 Dual problem of TE optimization

In this section, we present the dual problem of the primal problem defined by Equation (1), The dual function  $g(\lambda)$  is defined as the infimum of the Lagrangian  $L(\mathcal{R}, m, \lambda)$  with respect to the primal decision variables  $\mathcal{R}$  and  $m$ :  $g(\lambda) = \inf_{\mathcal{R}, m} L(\mathcal{R}, m, \lambda)$ .

(i) Minimization with Respect to  $m$ : The Lagrangian contains the following term involving  $m$ :

$$\left(1 - \sum_{e \in E} \lambda_e c(e)\right) m.$$

To ensure the dual function  $g(\lambda)$  remains bounded, we analyze the behavior of this term in the following cases:

- If  $1 - \sum_{e \in E} \lambda_e c(e) > 0$ , the term  $(1 - \sum_{e \in E} \lambda_e c(e))m$  becomes unbounded as  $m \rightarrow -\infty$ , causing  $L(\mathcal{R}, m, \lambda)$  to diverge to  $-\infty$ . This makes the dual problem infeasible.
- If  $1 - \sum_{e \in E} \lambda_e c(e) < 0$ , the term becomes unbounded as  $m \rightarrow +\infty$ , leading to a similar divergence of  $L(\mathcal{R}, m, \lambda)$  to  $-\infty$ .
- Therefore, the only feasible case is when:  $1 - \sum_{e \in E} \lambda_e c(e) = 0$

(ii) Minimization with Respect to  $\mathcal{R}$ : The part of the Lagrangian involving  $\mathcal{R}$  is given by:

$$\sum_{s,t \in V} \sum_{p \in P_{st}} \sum_{e \in p} \lambda_e D_{st} r_p.$$

Minimizing this term with respect to  $\mathcal{R}$  must satisfy the primal constraints  $r_p \geq 0$  and  $\sum_{p \in P_{st}} r_p = 1$ . As analyzed in §4.2, this is minimized when all the weight is placed on the path  $p \in P_{st}$  with the smallest  $\sum_{e \in p} \lambda_e$ .

(iii) In summary, the dual problem is shown in Equation (18).

$$\begin{array}{ll} \text{maximize}_{\lambda} & \sum_{s,t \in V} D_{st} \left( \min_{p \in P_{st}} \left( \sum_{e \in p} \lambda_e \right) \right) \\ \text{subject to} & 1 - \sum_{e \in E} \lambda_e c(e) = 0, \\ & \lambda_e \geq 0, \forall e \in E. \end{array} \quad (18)$$

## C ADDITIONAL DETAILS

### C.1 Details of self-attention

In this section, we briefly introduce the computation process of self-attention and explain why using transformers to obtain path embeddings generates intermediate variables whose size is proportional to the square of the path length.

The self-attention mechanism processes an input sequence  $X \in \mathbb{R}^{l \times d}$ , where  $l$  is the sequence length and  $d$  is the feature dimension, to compute a weighted output that captures contextualized representations of each position in the sequence. The process involves several steps:

**1. Projection into Query, Key, and Value:** The input  $X$  is transformed into three learned representations: Query ( $Q$ ), Key ( $K$ ), and Value ( $V$ ). These are computed as:  $Q = XW_Q$ ,  $K = XW_K$ ,  $V = XW_V$ , where  $W_Q, W_K, W_V \in \mathbb{R}^{d \times d_k}$  are learnable projection matrices, and  $Q, K, V \in \mathbb{R}^{l \times d_k}$ .

**2. Computing the Attention Matrix:** To model the relationships between all sequence positions, pairwise similarity scores between  $Q$  and  $K$  are calculated using a scaled dot-product:

$$A = \text{Softmax}\left(\frac{QK^T}{\sqrt{d_k}}\right), \quad (19)$$

where  $A \in \mathbb{R}^{l \times l}$  represents the attention weights. Each entry in  $A$  reflects the importance of one sequence position to another, normalized using the softmax function.

**3. Weighted Summation with the Value Matrix** The attention matrix  $A$  is then multiplied with the Value matrix  $V$  to compute the final output.

The intermediate variable that grows with the square of the Path length is generated during the computation of the attention matrix, given that the sequence length in HARP is equal to the Path length.

## C.2 Influence of topology variation

We find that any topology variations can be reflected in the path-to-edge matrix and the edge capacity vector. To demonstrate this, we first reformulate the calculation from  $\mathcal{R}$  to MLU using Equation (20), performing the calculation in matrix form. We define  $\Phi$  as the set of all paths, expressed as  $\Phi = \bigcup_{s,t \in V} P_{st}$ . The matrix  $\xi^{(|\Phi|,|E|)}$ , referred to as the Path-to-Edge matrix, specifies whether a given path  $i$  includes edge  $j$ . Here,  $\xi_{ij} = 1$  if edge  $j$  is part of path  $i$ , and 0 otherwise. The vector  $DM^{(|\Phi|,1)}$  represents the path's serving source-destination pair's demand, obtained by replicating each entry of the flattened traffic matrix  $K$  times. The vector  $\mathcal{R}^{(|\Phi|,1)}$  represents the TE configurations. The vector  $C^{(|E|,1)}$  represents the edge capacities. The symbol  $\times$  denotes matrix multiplication, and  $\odot$  indicates element-wise multiplication.

$$MLU = \max(\xi^T \times (DM \odot \mathcal{R})) / C. \quad (20)$$

From Equation (20), we find that in the TE optimization problem, there are two quantities related to topology. The first is the Path-to-Edge matrix  $\xi$ , and the second is the capacity vector  $C$ . Any type of 'variable' actually ultimately reflects changes in these two quantities.

- Variables in Node/Edge. 1) The addition and removal of nodes lead to changes in the source-destination pairs, thereby altering the path set  $\Phi$ , which changes the first dimension ( $|\Phi|$ ) of the Path-to-Edge matrix  $\xi$ . 2) The addition and removal of edges change the length of the capacity vector  $C$  and the second dimension ( $|E|$ ) of the matrix  $\xi$ . Additionally, these changes may alter the tunnels, that is, the edges that paths traverse, changing the locations of the '1' values within the matrix  $\xi$ . 4) Reordering of edge IDs results in permutation in capacity vector  $C$  and column permutation in matrix  $\xi$ . 5) Reordering node IDs alters the order within source-destination pairs and the traffic matrix, resulting in a permutation of associated paths in matrix  $\xi$ .
- Variables in Path. 1) Re-selection of paths results in changing the locations of the '1' values within the matrix  $\xi$ . 2) Reordering of path IDs within a source-destination pair corresponds to row permutation in the matrix  $\xi$ .
- Variables in Capacity leads to changes in the capacity vector  $C$ .

## C.3 Pseudocode for adjusting dual variable

We demonstrate how to adjust the dual variable  $\lambda$  in Pseudocode 1. Our input also includes an additional term,  $\lambda_e$ , as it helps the neural network determine the magnitude of  $\Delta\lambda_e$  based on the value of  $\lambda_e$ , which is equivalent to selecting an appropriate step size in the gradient descent process. The detailed of Softmin Operation in Line 4 is as follows:

---

### Pseudocode 1: Adjust dual variable $\lambda$

---

**Input:** Path-to-Edge matrix  $\xi^{(|\Phi|,|E|)}$ , Capacity vector  $C^{(|E|,1)}$ , Path traffic demand  $DM^{(|\Phi|,1)}$ , Initial dual variable  $\lambda^{(|E|,1)}$ , Number of adjustment iteration  $L$ , Number of source-destination Paris  $|\Omega|$ , Number of paths per pair  $K$ .

**Output:** Adjusted dual variable  $\lambda^{(|E|,1)}$ .

- 1 Let  $\mathcal{N}$  be a neural network with input dimension 4 and output dimension 1.
  - 2 **for**  $i$  in  $0, 1, \dots, L$  **do**
  - 3     Sum lambda on path  $\Lambda^{(|\Phi|,1)} = \xi^{(|\Phi|,|E|)} \times \lambda^{(|E|,1)}$ ;  
    //  $\Lambda_{\text{reshape}}^{(|\Omega|,K)}$  is the reshaped form of  $\Lambda^{(|\Phi|,1)}$ .  
    The Softmin operation is applied along the last dimension. For a detailed explanation of the Softmin operation, please refer to Appendix C.3.
  - 4     TE configuration  $\mathcal{R}_{\text{reshape}}^{(|\Omega|,K)} = \text{Softmin}(\Lambda_{\text{reshape}}^{(|\Omega|,K)})$ ;
  - 5     Flow on edge  $\mathcal{E}^{(|E|,1)} = \xi^T \times (DM^{(|\Phi|,1)} \odot \mathcal{R}^{(|\Phi|,1)})$ ;
  - 6     MLU  $m = \max(\mathcal{E}^{(|E|,1)} / C^{(|E|,1)})$ ;  
    //  $m_{\text{repeat}}$  is the repetition of  $m$  for  $|E|$  times. The Concatenate operation is performed along the last dimension.
  - 7     Neural Network Input  $\mathcal{I}^{(|E|,4)} =$   
       Concatenate( $\mathcal{E}^{(|E|,1)}, C^{(|E|,1)}, \lambda^{(|E|,1)}, m_{\text{repeat}}$ );
  - 8      $\Delta\lambda^{(|E|,1)} = \mathcal{N}(\mathcal{I}^{(|E|,4)})$ ;
  - 9      $\lambda^{(|E|,1)} = \lambda^{(|E|,1)} + \Delta\lambda^{(|E|,1)}$ ;
  - 10 **end**
  - 11 **return**  $\lambda^{(|E|,1)}$
- 

Softmin is a commonly used mathematical operation typically applied to tasks such as normalization or weight assignment in deep learning. The Softmin operation assigns larger weights to smaller input values and smaller weights to larger input values.

Formula: Given an input vector  $x = [x_1, x_2, \dots, x_n]$ , the output of the Softmin operation is computed as:

$$y_i = \frac{e^{-x_i}}{\sum_{j=1}^n e^{-x_j}}. \quad (21)$$

Characteristics:

- **Normalized output:** Softmin operation ensures that the output is always greater than 0 and the sum of the outputs equals 1. This satisfies the constraints in Equation (7).
- **Smaller input values correspond to larger output weights:** Due to the negative exponent, Softmin maps smaller input values to larger weights. This aligns with the requirements of the objective function in Equation (7).

Due to these two properties, which align perfectly with the requirements of Equation (7) for deriving the TE configuration  $\mathcal{R}$  from the dual variable  $\lambda$ , and given that Softmin, unlike the min function, is differentiable and thus facilitates training in deep learning, we choose the Softmin operation as the mapping function from  $\lambda$  to  $\mathcal{R}$ .

#### C.4 Traffic matrix partitioning illustration

Figure 13 illustrates an example of traffic matrix partitioning in a topology with 3 nodes and 6 source-destination pairs. As shown in the figure, the topology remains unchanged, while only the source-destination pairs are partitioned.

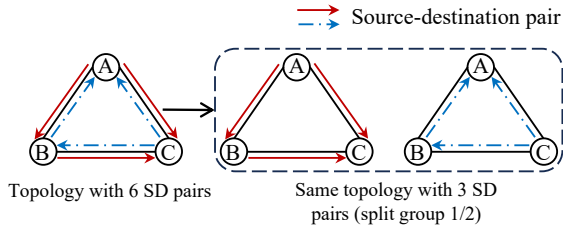


Figure 13: Traffic matrix partitioning ( $S = 2$ ).

#### C.5 Evaluation setup

Our evaluation setup is as follows: The experiments are conducted using Ubuntu 18.04, an Intel Xeon Silver 4110 CPU at 2.10 GHz, and 128 GiB RAM. The programming is carried out using Python 3.8, and the deep learning framework employed is PyTorch, version 2.4.0. The default GPU used is the NVIDIA Tesla P100-PCIE with 16 GiB of VRAM, running CUDA version 11.8. However, due to the high GPU memory demands of TE schemes like HARP, some topologies cause ‘Out of Memory’ (OOM) errors when tested on the Tesla P100-PCIE. Additionally, as analyzed in §2.2, HARP is challenging to parallelize across multiple GPUs. Consequently, for these cases, we have to use the advanced A100-SXM4-80GiB GPU with 80 GiB. To ensure consistency, all throughput results obtained on the A100-SXM4-80GiB are normalized to align with the computation speed of the Tesla P100-PCIE, based on the proportional difference in processing speed between the two GPUs. We use the Tesla P100-PCIE as the primary GPU to showcase that even on a standard GPU, our approach remains both effective and practical.

#### C.6 Hyperparameter Search

For DOTE, our hyperparameter search considers a learning rate of (1e-4, 1e-3), the number of hidden layers (2, 3, 4), and a hidden dimension of (128, 256). FIGRET shares the same architectural hyperparameters as DOTE, with an additional

robustness-enhancing loss function, for which we set the weight to 0.1.

For TEAL, we explore a learning rate of (1e-5, 1e-4, 5e-4, 1e-3), FlowGNN layers (6, 8), and (5, 10) samples for reward estimation. In addition to hyperparameters, we find that normalizing the input traffic matrix and link capacities improves performance [7]. To achieve this, we experiment with multiple renormalization factors. Moreover, TEAL’s primary objective is to maximize the total feasible flow, meaning the total traffic that can be accommodated without exceeding link capacities. As a result, the split ratios for a given source-destination pair do not necessarily sum to 1, reflecting uncollected traffic. However, in MLU optimization, this constraint is required. To align TEAL with MLU optimization, we introduce a minor adjustment to its formulation.

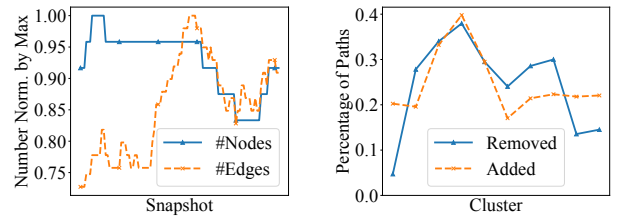
For HARP, we search over a learning rate of (1e-4, 1e-3, 7e-3), the number of RANs (3–10), GNN layers (1, 2, 4), and Transformer layers (1, 2).

For RedTE, we follow all hyperparameter settings specified in its source code [1], including random seed and reinforcement learning parameters such as epsilon step, explore decay, and others. For complete details, please refer to [1].

For Geminet, we consider a learning rate of (1e-4, 7e-3), the number of iterative adjustments (3–10), and two MLP components: MLP1 in the Initial Dual Variable Generation Module with (2, 3, 4, 5) layers and MLP2 in the Adjustment Module with (1, 2) layers.

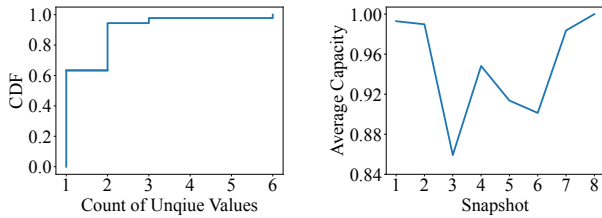
#### C.7 Details of DynGeant

In this section, we present the topological variations of DynGeant. The topological variations across clusters and within clusters are depicted in Figure 14 and Figure 15, respectively.



(a) Variation in the number of nodes/edges per snapshot (normalized to the maximum number of nodes across snapshots). (b) Changes in Paths across Clusters: Analysis of path additions and removals in clusters at every 5-cluster interval.

Figure 14: Topology variations across clusters in the DynGeant.



(a) Number of unique capacity values per link across snapshots of the last cluster. (b) Average capacity across snapshots of the last cluster.

**Figure 15: Topology variations across snapshots within the last cluster in the DynGeant.**

## D ADDITIONAL RESULTS

### D.1 Sparse Multiplication in PyTorch

In Listing 1, we show the GPU memory usage of sparse matrix multiplication in PyTorch. Taking the KDL topology as an example, the topology consists of 754 nodes and 1790 edges. Each source-destination pair has 4 paths, resulting in a total of  $754 \times 753 \times 4 = 2271048$  paths. The Path-to-Edge matrix for KDL has a shape of (2271048, 1790), with a total of 53902044 non-zero elements. When a sparse tensor shaped like the Path-to-Edge matrix and a dense tensor representing the flow on paths are loaded into the GPU, the memory usage and peak memory consumption are both 1.14 GiB. After performing sparse matrix multiplication, the memory usage remains 1.14 GiB (as the tensor  $t$  of shape (16, 1790) is relatively small), but the peak memory consumption increases to 4.35 GiB. It can be observed that the peak memory usage significantly exceeds the combined sizes of the sparse and dense matrices. The purpose of this section is to report this phenomenon and provide additional explanations to the data presented in Table 1. This phenomenon is related to the implementations of Pytorch and the CUDA sparse matrix library<sup>1</sup>, which are beyond the scope of our optimization considerations.

Following the method described in §4.4, dividing the group into four parts ( $S = 4$ ) results in a new shape for the Paths to Edge matrix of (567762, 1790). For convenience in the example, we take the number of nonzeros as one-fourth of the original, which is now 13475511. After updating the respective values and rerunning the code from Listing 1, the final peak memory usage becomes 1.09 GiB. Compared to the initial 4.35 GiB, this represents a reduction of approximately  $\left(\frac{4.35-1.09}{4.35}\right) \approx 75.17\%$ , vividly illustrating the benefits of partitioning source-destination pairs. We present a more comprehensive evaluation in §5.5, demonstrating that this method of training on sub-pairs can reduce memory

<sup>1</sup><https://docs.nvidia.com/cuda/cusparse/index.html#cusparsespm>

consumption and increase throughput while maintaining performance comparable to training on entire pairs.

```

1 import torch
2
3 shape = (2271048, 1790) # shape of KDL's
4   Paths to Edges matrix
5 num_nonzero = 53902044 # number of non-zero
6   elements in the Paths to Edges matrix
7 batch_size = 16
8
9 rows = torch.randint(0, shape[0], (
10   num_nonzero,))
11 cols = torch.randint(0, shape[1], (
12   num_nonzero,))
13 values = torch.rand(num_nonzero)
14
15 indices = torch.stack([rows, cols])
16 sparse_tensor = torch.sparse_coo_tensor(
17   indices, values, size=shape).cuda() #
18   Shape like Paths to Edges matrix, (
19   num_paths, num_edges)
20 dense_tensor = torch.rand(batch_size, shape
21   [0]).cuda() # Shape like flow on paths,
22   (batch_size, num_paths)
23 print(f'GPU memory usage: {torch.cuda.
24   memory_allocated()/1024**3} GiB') # 1.14
25   GiB
26 print(f'GPU max memory usage: {torch.cuda.
27   max_memory_allocated()/1024**3} GiB') #
28   1.14 GiB
29 t = torch.sparse.mm(dense_tensor,
30   sparse_tensor)
31 print(f'GPU memory usage: {torch.cuda.
32   memory_allocated()/1024**3} GiB') # 1.14
33   GiB
34 print(f'GPU max memory usage: {torch.cuda.
35   max_memory_allocated()/1024**3} GiB') #
36   4.35 GiB

```

**Listing 1: Code for sparse matrix multiplication in PyTorch demonstrating GPU memory usage**

### D.2 DOTE vs. Dual DOTE

In this section, we apply duality theory to DOTE by modifying its final layer to output dual variables, demonstrating that our duality-based approach is extendable to other TE schemes. We summarize the memory usage results in Figure 16. The performance results are summarized in Table 4. It can be observed that Dual DOTE significantly reduces memory consumption by substantially decreasing the size of the neural network’s output layer.

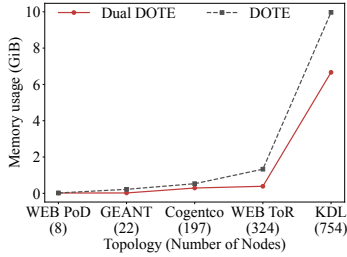


**Figure 16: Comparison of memory usage between Dual DOTE and DOTE.**

Topology name	WEB PoD	GEANT	Cogentco	WEB ToR	Kdl
Performance Ratio	1.01	1.02	0.99	1.02	0.99

**Table 4: Result of the performance of Dual DOTE, where the performance ratio refers to the average normalized MLU of Dual DOTE divided by the average normalized MLU of DOTE.**

### D.3 Number of model parameters

In this section, we delve into the analysis of the number of neural network model parameters across different ML-based TE schemes, with the results summarized in Figure 5(a). Figure 5(a) is based on the scenario where each source-destination pair has 4 paths. For FIGRET, the neural network model it uses is the same as that used by DOTE. From the results, we can draw the following conclusions:

- For Geminet, HARP, and TEAL, as long as certain topology-independent hyperparameters (e.g., the number/dimensions of hidden layers) remain unchanged, the size of their neural network models is independent of the topology. This is because, in the case of Geminet, HARP, and TEAL, their MLPs are designed to process edges, paths, or source-destination pairs individually, rather than accounting for the entire topology. Moreover, the graph neural networks used by TEAL and HARP also have parameter sizes that are independent of the graph’s scale. On the other hand, DOTE uses an MLP whose input depends on the total number of source-destination pairs and whose output depends on the total number of paths. As a result, its model parameters increase as the topology grows.
- The number of parameters in Geminet is significantly smaller than in the other three methods. For instance, on GEANT, the number of parameters in Geminet is only 0.07 of TEAL, 0.026 of HARP, and  $4 \times 10^{-4}$  of DOTE. Having fewer parameters offers advantages: i) requiring less memory to store the model, ii) smaller models typically require less data for training, iii) being less prone to overfitting, and iv) exhibiting better generalization performance.

### D.4 Additional performance results

This section presents additional performance results evaluated on the one-cluster topologies. This includes results on the PoD-level Meta WEB topology (Figure 17) and on the KDL topology (Figure 18). In Figure 18, considering the low throughput of HARP and TEAL on KDL, which results in long training times, our results only include Geminet and DOTE. However, this does not affect our conclusion: on the original tunnels, Geminet performs on par with any ML-based TE scheme and can handle tunnel shuffle.

### D.5 Interpreting of training on sub-tms

In this section, we visualize the distribution of the input values and the parameters of the neural network models. Figure 19 shows the distribution of relative link utilization (edge utilization divided by MLU) before and after partitioning. It can be observed that partitioning has little impact on the distribution of relative link utilization. As analyzed in §4.4, Geminet relies on relative link utilization rather than absolute edge loads for training. Since partitioning does not alter the relative utilization distribution, it does not affect the final training performance.

To further validate this, we visualize the trained neural network parameters. Figure 20 compares the model of the non-partitioned baseline with the model trained on one group after partitioning into 8 groups for the KDL topology. The neural networks consist of three layers: an input layer, a hidden layer, and an output layer. The weight matrices of these three layers are visualized. From the results, it can be observed that the parameters of the trained neural networks are relatively similar. The cosine similarity is 97%.

### D.6 Training on all groups

Figure 21 summarizes the performance results when training with all partitioned groups. From the results, it can be observed that training with all partitioned groups performs as well as the non-partitioned baseline. On the WEB ToR topology, the performance drops compared to the non-partitioned baseline for  $S = 2$ ,  $S = 4$ , and  $S = 8$  are  $-0.7\%$ ,  $-0.1\%$ , and  $-0.8\%$ , respectively. For the KDL topology, the corresponding values are  $0.1\%$ ,  $0.1\%$ , and  $-0.1\%$ . Negative values indicate an improvement rather than a drop in performance.

Regarding why the performance improves, our initial investigation suggests that when the data is partitioned into  $s$  groups, it adds  $s - 1$  additional groups of training data compared to the non-partitioned scenario. As discussed in §5.5, the edge relative load (edge utilization / Max Link Utilization) is more critical for adjustments. The additional  $s - 1$  groups of training data may expose the neural network to more diverse edge relative load scenarios, thereby enhancing the model’s ability to make adjustments.

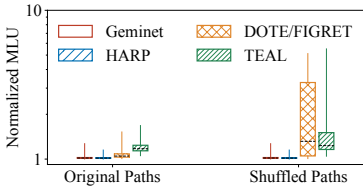


Figure 17: Comparing ML-based TE schemes for PoD-level Meta WEB.

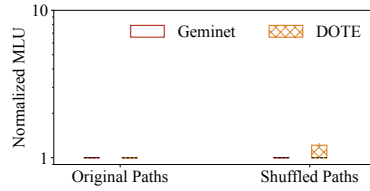


Figure 18: Comparing ML-based TE schemes for KDL topology.

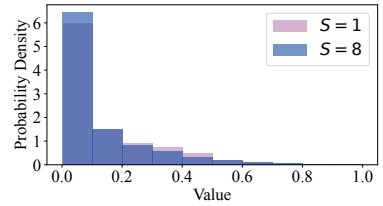


Figure 19: The distribution of edge utilization divided by MLU.

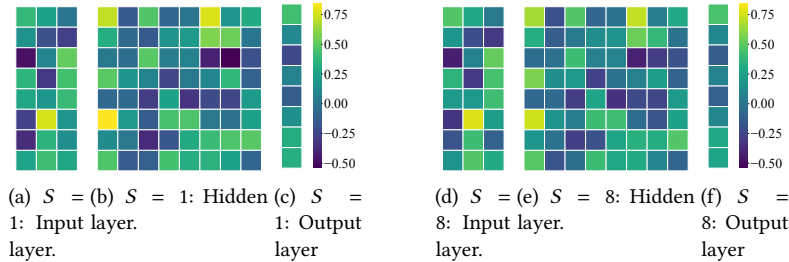


Figure 20: Comparison of the neural network parameters between the non-partitioned baseline  $S = 1$  and the model trained with partitioning into 8 groups  $S = 8$  (using only one group for training) on KDL. The neural network takes an input of dimension 3 ( $\lambda_e$ , edge capacity, edge utilization divided by MLU), has one hidden layer of dimension 8, and an output layer of dimension 1 ( $\Delta\lambda_e$ ). Thus, there are three weight matrices in total: input layer ( $3 \times 8$ ), hidden layer ( $8 \times 8$ ), and output layer ( $8 \times 1$ ). For better visualization, the input layer weight matrix has been transposed. The trained neural network exhibits highly similar parameters.

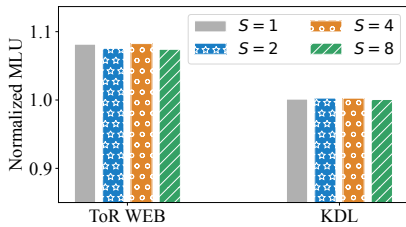


Figure 21: Changes in average normalized MLU with the number of partitions ( $S$ ) when training with all partitioned groups.

### D.7 Additional link failure results

In this section, we present the results from evaluating link failures on PoD-level Meta WEB and ToR-level Meta WEB, as shown in Figure 22 and Figure 23.

From the results, it can be observed that Geminet performs on par with HARP across WAN topologies, data center PoD-level, and ToR-level topologies. Additionally, methods capable of handling variable topologies, such as Geminet and HARP, consistently outperform DOTE in addressing link failures.

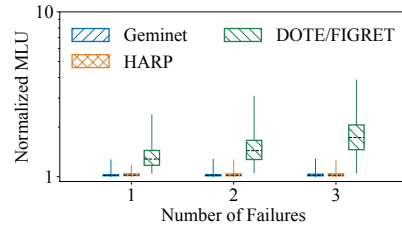


Figure 22: Coping with different numbers of random link failures on PoD-level Meta WEB.

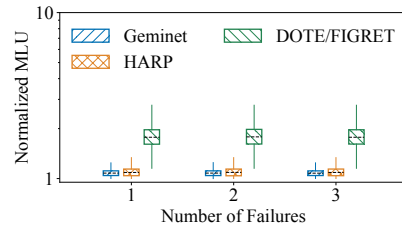


Figure 23: Coping with different numbers of random link failures on ToR-level Meta WEB.